

**Joint Development of  
Seismic Capability Evaluation Technology  
for Degraded Structures and Components**

**Annual Report for Year 2 Task**

**Identification and Assessment of  
Material Models for Age-Related Degradation of  
Structures and Passive Components in  
Nuclear Power Plants**

March 2009

Jinsuo Nie, Joseph Braverman, and Charles Hofmayer  
Brookhaven National Laboratory  
Upton, NY 11973, USA

Min Kyu Kim and In-Kil Choi  
Korea Atomic Energy Research Institute  
Daejeon, 305-353, Korea



## **NOTICE/DISCLAIMER**

This manuscript has been authored by employees of Brookhaven Science Associates, LLC under Contract No. DE-AC02-98CH10886 with the U.S. Department of Energy. The United States Government retains a non-exclusive, paid-up, irrevocable, world-wide license to publish or reproduce the published form of this manuscript, or allow others to do so, for United States Government purposes.

Neither the United States Government nor any agency thereof, nor any of their employees, nor any of their contractors, subcontractors, or their employees, makes any warranty, express or implied, or assumes any legal liability or responsibility for the accuracy, completeness, or any third party's use or the results of such use of any information, apparatus, product, or process disclosed, or represents that its use would not infringe privately owned rights. Reference herein to any specific commercial product, process, or service by trade name, trademark, manufacturer, or otherwise, does not necessarily constitute or imply its endorsement, recommendation, or favoring by the United States Government or any agency thereof or its contractors or subcontractors. The views and opinions of authors expressed herein do not necessarily state or reflect those of the United States Government or any agency thereof.

## ABSTRACT

When performing seismic safety assessments of nuclear power plants (NPPs), the potential effects of age-related degradation on structures, systems, and components (SSCs) should be considered. To address the issue of aging degradation, the Korea Atomic Energy Research Institute (KAERI) has embarked on a five-year research project to develop a realistic seismic risk evaluation system which will include the consideration of aging of structures and components in NPPs. Three specific areas that are included in the KAERI research project, related to seismic probabilistic risk assessment (PRA), are probabilistic seismic hazard analysis, seismic fragility analysis including the effects of aging, and a plant seismic risk analysis.

To support the development of seismic capability evaluation technology for degraded structures and components, KAERI entered into a collaboration agreement with Brookhaven National Laboratory (BNL) in 2007. The collaborative research effort is intended to continue over a five year period with the goal of developing seismic fragility analysis methods that consider the potential effects of age-related degradation of SSCs, and using these results as input to seismic PRAs. In the Year 1 scope of work BNL collected and reviewed degradation occurrences in US NPPs and identified important aging characteristics needed for the seismic capability evaluations that will be performed in the subsequent evaluations in the years that follow. This information is presented in the Annual Report for the Year 1 Task, identified as BNL Report-81741-2008 and also designated as KAERI/RR-2931/2008. The report presents results of the statistical and trending analysis of this data and compares the results to prior aging studies. In addition, the report provides a description of U.S. current regulatory requirements, regulatory guidance documents, generic communications, industry standards and guidance, and past research related to aging degradation of SSCs.

This report describes the research effort performed by BNL for the Year 2 scope of work. This research focused on methods that could be used to represent the long-term behavior of materials used at NPPs. To achieve this BNL reviewed time-dependent models which can approximate the degradation effects of the key materials used in the construction of structures and passive components determined to be of interest in the Year 1 effort. The intent was to review the degradation models that would cover the most common time-dependent changes in material properties for concrete and steel components.



## TABLE OF CONTENTS

ABSTRACT .....	iii
List of Tables .....	vi
List of Figures .....	vi
1 INTRODUCTION .....	1
2 SCOPING STUDY OF MATERIALS AND COMPONENTS .....	3
2.1 General Observations .....	3
2.2 Risk Significant Structures and Passive Components .....	4
2.3 Identification of Dominant Materials .....	5
3 DEGRADATION MODELS FOR CONCRETE .....	19
3.1 Overview of Cracking and Corrosion .....	20
3.1.1 Effects of Crack Characteristics on Corrosion .....	20
3.1.2 Effects of Corrosion on Crack Characteristics .....	21
3.2 The Power Model .....	21
3.3 Thoft-Christensen's Model .....	23
3.3.1 Time for Corrosion Initiation by Chloride Penetration .....	23
3.3.2 Corrosion of Reinforcement .....	24
3.3.3 Initiation of Cracking .....	24
3.3.4 Corrosion Crack Evolution .....	26
3.4 Basheer's Model .....	26
3.4.1 Transport Model for Chloride Ions .....	27
3.4.2 Corrosion Model .....	27
3.4.3 Structural Model .....	28
3.5 Sarveswaran's Model .....	28
3.6 Marsh's Model .....	28
4 DEGRADATION MODELS FOR CARBON AND LOW-ALLOY STEELS .....	33
4.1 The Power Model .....	33
4.2 Henshall's Model (Dry Oxidation) .....	33
4.3 Fatigue Crack Growth Models .....	35
4.4 Corrosion-Modified Fatigue Crack Growth Models .....	36
4.5 Corrosion Models .....	37
5 DEGRADATION MODELS FOR STAINLESS STEEL .....	41
5.1 Machida's Model .....	41
5.1.1 Model for Crack Initiation .....	41
5.1.2 Crack Growth Models .....	41
5.2 Time-Dependent Fatigue Damage Model .....	42
5.3 Mechanochemical Model for SCC in High Temperature Water .....	43
6 OBSERVATIONS AND CONCLUSIONS .....	47
7 REFERENCES .....	49

**LIST OF TABLES**

Table 2-1 Summary of Materials and Their Intended Functions and Subcomponents ..... 7  
Table 2-2 Dominant Materials for Selected Components ..... 14  
Table 3-1 Relationship between Surface Crack Width and Corrosion Depth/Length [Beeby, 1979]..... 31  
Table 3-2 Time to Develop Visible Crack in Concrete Cover vs Corrosion Rate [Andrade, Alonso, and Molina, 1993]..... 31  
Table 4-1 Average Values for Corrosion Parameters  $C$  and  $\alpha$  [Albrecht and Naemi, 1984]..... 40

**LIST OF FIGURES**

Figure 2-1 Distribution Comparison of SPC Degradation Occurrences over Component..... 17  
Figure 2-2 Comparison of Normalized Distribution of SPC Degradation Occurrences over Component ..... 17

# 1 INTRODUCTION

## Year 2 Objectives:

The Year 2 research objective is to identify modeling methodologies to represent the long-term behavior of materials used in nuclear power plants (NPPs). Depending on the particular component, material, environment, and loading, such time-dependent material degradation models may be used in conjunction with probabilistic risk assessments (PRAs) to estimate the time it would take for degradation of a component to introduce significant risk to a NPP.

## Approach:

Based on past experience, developing time-dependent degradation models is considered to be extremely complex, very much component/material dependent, environment dependent (e.g., temperature, moisture, radiation), load (stress) dependent, and would be a significant undertaking. In order to simplify the process, this research effort relied on the available information that can be identified in the literature both in the US and other nations, in the nuclear industry and other industries; thereby providing a cost effective means to achieve the stated goal. The level of success of this effort, therefore, depends to a large extent on the available information that can be identified.

The approach used in this research effort was to collect and review other studies in the open literature in order to identify time-dependent material models which can approximate the degradation effects of the key materials used in the construction or fabrication of the structures and passive components determined to be of interest from the Year 1 effort. It is envisioned that the degradation models identified would potentially cover the most common time-dependent changes in material properties (e.g., strength, ductility, modulus), loss of material (e.g., corrosion, erosion), and cracking. The time-dependent degradation models may be in the form of a mathematical equation as a function of one or more parameters, statistical data from operating experience, or test results.

## Report Organization:

The annual report for the Year 2 task comprises of 7 sections including one for References. Section 2 of this report presents a scoping study that identifies risk-significant components and their dominant materials, which are used in later sections for identifying the time-dependent degradation models. Sections 3 through 5 provide descriptions of the identified degradation models, with an emphasis on concise summaries of the essential formulations, tables, important parameters, and special considerations for the application of these models in fragility analysis. Section 3 is devoted to the concrete material, the most common material in NPP construction. A discussion of the relationship of concrete crack characteristics and reinforcement corrosion is also presented in Section 3. Section 4 presents a summary of degradation models for carbon and low-alloy steels, and Section 5 presents degradation models for stainless steel. Conclusions and important observations are presented in Section 6.



## 2 SCOPING STUDY OF MATERIALS AND COMPONENTS

### 2.1 General Observations

Age-related degradations of structures and passive components (SPCs) in nuclear power plants (NPPs) are highly complex processes that may depend on material specification, fabrication and construction, normal and abnormal loading conditions, environment, maintenance programs, and many other factors. Encapsulating all or most of these factors in time-dependent degradation models is essentially impractical. Most models found in the literature (to be presented in later sections) have their emphasis on some particular degradation factors. However, omitting some factors in these models does not necessarily represent significant drawbacks in their practical applicability because the factors contributing to SPC degradations usually do not exist coincidentally for any particular case. Therefore, it is extremely important that the use of any of these models in the development of seismic capability evaluation technologies must be under careful scrutiny, with regard to the components in question and their associated factors such as loading conditions, environment (e.g., temperature, moisture, or irradiation), and failure modes.

The difficulty in developing age-related degradation models for SPCs also lies in the difficulty in identification of SPCs that are potentially significant in plant safety. This point is often not obvious at first glance. As the number of different SPCs is relatively large, developing or identifying age-related degradation models for all of these SPCs are prohibitive, and therefore such effort must be restricted to those SPCs that are most significant in affecting plant safety. However, identification of safety-significant SPCs is difficult as well. SPCs with higher degradation occurrences may not necessarily imply significant risks to the plant safety, because these components may be under active inspection/maintenance programs or their degradation may not be safety-related at all. On the other hand, some SPCs that are subject to slow degradation or not under regular maintenance may impose substantial risk to the plant safety, especially for those components that are vulnerable to low probability high consequence initiating events, such as large earthquakes.

In developing/identifying degradation models for selected SPCs, the ultimate use of these models, to be utilized in the later stage of this multi-year research program, must be considered in order to maximize the usefulness of these models. In particular, since the degradation models will be used in the development of fragility models that may consider time dependent degradation effects, dominant failure modes of these SPCs that define the limit states for the fragility models must be envisioned during the identification and documentation of the time-dependent degradation models for the selected SPCs. As multiple failure modes may contribute to a common limit state for a particular fragility model, selection of appropriate models for degradation can be very difficult because the degradation models available in the literature are less likely to include all failure modes in the domain of fragility analysis. Therefore, integration of models from different sources and the associated justification of such integration will be very important.

The time-dependent degradation models can be in the form of mathematical formulations, statistical data from operating experience, or test results. These models will be documented with the background information, the description of the models, and assessment of the applicability for fragility analysis.

The effort in identification/development of the degradation models relies on publicly available information sources for cost effectiveness and schedule considerations. Since the required models may not be readily available from documents related to NPP SPCs, sources from other industries may also be used.

This section of the research report presents a scoping study that comprises identification of SPCs that are safety significant to NPPs and identifications of the dominant materials for the selected SPCs.

## **2.2 Risk Significant Structures and Passive Components**

The Year 1 annual report (BNL Report-81741-2008, also designated as KAERI/RR-2931/2008 [Nie, 2008]) presents a survey of the degradation occurrences using the Licensee Event Reports (LERs) and developed statistics on the distribution of these degradation occurrences over various controlling parameters. Utilizing the same figures from the Year 1 annual report for convenience, Figure 2-1 shows the distribution of SPC degradation occurrences as a function of component type (category of component). This figure was developed using data from LER 1999-2008, NUREG/CR-6679 [Braverman, et. al., 2000], and LER 1985-1997 (from NUREG/CR-6679). Figure 2-2 shows the same three data series that were normalized by the total number of degradation occurrences for each data series. Except for data series from LER 1985-1997, that explicitly excluded many piping components, these two figures show that the top three component categories having the greatest number of degradation occurrences are exchangers, piping systems, and reactor pressure vessels (RPVs). The somewhat large variations between these two series and the LER 1985-1997 may be originated from the differences in the methods for determination of the degradation occurrences and in other possible biases in various aspects of data collection and processing, as discussed in the Year 1 Annual Report. However, the top three component categories, identified as exchangers, piping systems, and RPVs, can be accepted as the most vulnerable components based on the degradation occurrences.

The collection of degradation occurrences of SPCs during Year 1 also revealed that structural type components, i.e., containments, structural steel, concrete, and anchorages occurred only 18 times, about 8% of all degradation occurrences. However, this observation should not be considered as an indication that no significant degradations occurred in structures, but as an indication that the nature of the LER reporting system does not necessarily reflect the full scale of structural degradation. Since the LERs tend to report events mostly related to operating experiences having safety significance, structural degradations usually represent less immediate impact on plant safety, and are thus less likely to be observed and reported in LERs. Most structural degradations can be found in the literature that involves results from special inspection efforts and nuclear industry studies. For example, NUREG-1522 covers data obtained from walkdowns conducted at six plants [NUREG-1522, 1995]. Therefore, structural components should be considered appropriately when screening the materials of SPCs for the purpose of degradation model identification.

The SPCs that merit the most effort for research, including identification of age-related degradation models, should be those having the most risk significance to plant safety. The risk significance of an aged component depends on the level of its degradation (degradation occurrence frequency) and its contribution to the system risk (e.g. core damage frequency). A scoping study by convolving the degradation occurrences and the risk contribution over the SPCs can be very costly to perform. Therefore, the selection of the most risk significant SPCs must be based on available information in the literature.

NUREG/CR-6679 presents an extensive review of past research on aging, which included NUREG/CR-6415 on age-related degradation on active components, NUREG/CR-6425 on aging effects on seismic failures, NUREG/CR-6157 on aging risk assessment methods and applications, and other relevant NUREG/CR reports and documents. Beyond the evaluation of degradation occurrences, NUREG/CR-6679 also included a scoping study that was targeted at identifying those SPCs that should have the highest priority for further research related to aging. This

prioritization was achieved by reviewing historical seismic PRAs, license renewal inspection reports, other NRC and industry requirements, and research studies related to aging. The NUREG/CR-6679 study aggregated information regarding the component's seismic risk significance, past degradation occurrences, importance to the licensing basis/license renewal, and adequacy of existing aging management programs. The study concluded that masonry walls, flat bottom steel tanks, anchorages, concrete, and buried piping were rated "high" using the various measures and deserved further research. Masonry walls were not included in the list of the ten component categories studied in this BNL/KAERI collaboration research effort, because safety related masonry walls are not commonly used in Korean NPPs.

Combining the results from the trending analysis of degradation occurrences and the results of the priority ranking from NUREG/CR-6679, exchangers, piping systems, RPVs, tanks, anchorages, and concrete are selected for use in identification of materials that will be used for identifying time-dependent models of aging-related degradation. It should be noted that although the list of these components does not cover all SPCs, the materials identified for these components are used extensively in the other components. Therefore, in most cases, the selected materials are representative for SPCs in general.

### **2.3 Identification of Dominant Materials**

Among these six component categories, concrete is already a specific material and does not require further screening. Concrete is an essential composite construction material used in many NPPs for their basemats, containments, neutron shielding, walls, slabs, and other structural components. Concrete structures and components are most important in resisting catastrophic disasters such as potential large earthquakes. Therefore, concrete is the first material to be examined in the next section.

For the four component categories, namely exchangers, piping systems, RPVs, and tanks, an effort in determining dominant materials used in these components was carried out by reviewing the License Renewal Applications (LRAs). LRAs, as required by 10 CFR Part 54 – the License Renewal Rule, contains scoping and screening information on structures, systems, and components (SSCs) subject to aging management review. LRAs mostly include a section for aging management review results, where for each major system a list of materials, environment, aging effects requiring management, and aging management programs are listed. Therefore, by reviewing these sections of the approved LRAs, the dominant materials for the selected risk significant SPCs can be determined.

Table 2-1 shows an extensive list of common materials used in the NPP SPCs and their intended functions (e.g. structural support, pressure boundary, and missile barrier) and the corresponding intended subcomponents (e.g. bolting, shroud support, and structural steel). For this information to be more useful in selecting the dominant materials, a connection to the selected component categories must be established. A second round review of the relevant tables in the approved LRAs focused on these specific component categories: exchangers, piping systems, RPVs, tanks, concrete, and structural steel (and other metallic materials). Table 2-2 shows the findings on the materials, environments, and aging effects requiring management that are associated with the selected component categories. It should be noted that the data listed in the review result tables in LRAs are not necessarily related to observed degradations but review results according to license review rules. It should be further noted that the materials listed in Table 2-2 do not represent an exact count of the number of occasions that a particular material has been used in NPPs. During the review of the LRAs, it has been found that stainless steel and carbon steel are the most widely used material for the majority of passive components, while the other listed materials may be used as cladding, fitting, nozzles, etc. Therefore, in addition to concrete, which was found to be

the most dominant structural material, stainless steel and carbon steel are selected for review of time-dependent age-related degradation models.

It should be pointed out that the selected component categories include an extremely large number of actual SPCs, which may fail in vastly different ways depending on their loading, environment, intended function, failure mode, and other factors. The environment and aging effect information in Table 2-2 provides typical scenarios for the purpose of identification of age-related degradation models. However, the application of the identified models to a SPC must be verified for its actual situation.

Although dominant materials for NPP SPCs are selected for identifying age-related degradation models, the materials themselves must often be placed in the context of components when discussing the degradation of these materials. Therefore, the models identified are mostly associated with certain components and their environments.

Table 2-1 Summary of Materials and Their Intended Functions and Subcomponents

<b>Material</b>	<b>Intended Function</b>	<b>Intended Subcomponent</b>
Low Alloy Steel	Mechanical Closure (MC)	1. Bolting
	Structural Support (SS)	1. Bolting 2. Shroud Support 3. Nozzle support pads
	Pressure Boundary (PB)	1. Ductwork 2. Fittings 3. Heat Exchangers 4. Piping 5. Traps 6. Valves 7. Strainers 8. Shroud Supports 9. Manway cover bolts 10. Closure head domes/flanges 11. Upper shells 12. Primary inlet/outlet nozzles 13. Intermediate Shells 14. Lower shells 15. Upper shell flanges 16. Closure studs, nuts and washers
	Fire Barrier (FB)	1. Fire Dampers
	Heat Transfer (HT)	1. Heat Exchangers
	Debris Protector (DP)	1. Strainers
	Carbon Steel	Fission Product Barrier (FPB)
Structural Support (SS)		1. Anchors/Bolts 2. Miscellaneous Steel 3. Reinforced Concrete 4. Structural Steel 5. Hangers/Supports for ASME Class I Piping 6. Cable Trays and Supports 7. Support skirts and flanges 8. Refueling seal ledges 9. Tube bundle wrappers 10. Wrapper supports 11. Support skirt integral attachments 12. Cranes 13. Retaining walls 14. EFWP Turbine casing 15. Battery Racks

<b>Material</b>	<b>Intended Function</b>	<b>Intended Subcomponent</b>
		16. Service Water Pump House (SWPH) 17. Main Condensers
	Radiation Shielding (RS)	1. Miscellaneous Steel 2. Reinforced Concrete 3. Structural Steel
	Pipe Whip Restraint	1. Miscellaneous Steel
	Missile Barrier (MB)	1. Reinforced Concrete 2. Structural Steel
	Pressure Boundary (PB)	1. Steel Bellows 2. Structural Steel 3. Reactor Coolant Pump 4. Motor upper bearing oil 5. Heat Exchanger 6. Channels and covers 7. Excess letdown Heat Exchanger tubes 8. Surge/Spray/Safety/Relief nozzle 9. Secondary closure covers 10. Emergency containment cooler headers 11. Emergency containment cooler housings 12. Valves Piping/fittings downstream 13. Valves Piping/fittings upstream 14. Refueling water storage tanks 15. Residual exchanger shells and baffles 16. Residual pump shells, covers, baffles 17. Emergency containment filter housings 18. Cleanout plugs 19. Instrument air system piping/tubing/valves 20. Diffusers
	Heat Transfer (HT)	1. Structural Steel 2. Excess letdown Heat Exchanger tubes
	Filtration	1. Debris screen gratings 2. Flow elements
Nickel Alloy	Mechanical Closure (MC)	1. Bolting
	Structural Support (SS)	1. Bolting 2. Shroud Supports 3. Penetrations
	Pressure Boundary (PB)	1. Flexible Connectors 2. Shroud Supports 3. Penetrations
	Fission Product Barrier (FPB)	1. Penetrations
Stainless Steel	Mechanical Closure (MC)	1. Bolting

Material	Intended Function	Intended Subcomponent
	Structural Support (SS)	<ol style="list-style-type: none"> <li>1. Bolting</li> <li>2. Fuel Supports</li> <li>3. Anchors/Bolts</li> <li>4. Reinforced Concrete</li> <li>5. Structural Steel</li> <li>6. Hangers/Supports for ASME Class I Piping</li> <li>7. Tube Trays and Covers</li> <li>8. Reactor Coolant pump lugs</li> <li>9. Tube support plates</li> <li>10. Main Condenser</li> </ol>
	Pressure Boundary (PB)	<ol style="list-style-type: none"> <li>1. Ductwork</li> <li>2. Fittings</li> <li>3. Flexible Connectors</li> <li>4. Piping</li> <li>5. Strainers</li> <li>6. Tubing</li> <li>7. Valves</li> <li>8. Penetrations</li> <li>9. Steel Bellows</li> <li>10. Structural Steel</li> <li>11. Orifices Reducers</li> <li>12. Primary loop elbows</li> <li>13. Excess letdown Heat Exchanger tubes</li> <li>14. Regenerative heat exchangers</li> <li>15. Surge/Spray nozzle thermal sleeve</li> <li>16. Instrument nozzles and Thermowells</li> <li>17. Surge/Spray/Safety/Relief nozzle safe ends</li> <li>18. Primary nozzle safe ends</li> <li>19. Control Rod drive mechanism rod travel houses</li> <li>20. Control Rod drive mechanism latch housing</li> <li>21. Control Rod drive mechanism housing flange</li> <li>22. Instrumentation tube/tube safe ends</li> <li>23. Bottom mount Instrumentation guide tubes</li> <li>24. Seal table fittings</li> <li>25. Primary nozzle safe ends</li> <li>26. Reactor coolant pumps</li> <li>27. Thermal Barrier heat exchanger tubes</li> <li>28. Exchanger nozzles</li> <li>29. Primary inlet/outlet lugs</li> <li>30. Inlet/outlet safe ends</li> <li>31. Containment Spray pumps</li> <li>32. Containment tube coil bands and clips</li> <li>33. Containment cyclone separators</li> <li>34. Valves Piping/Tubing fittings upstream/downstream</li> <li>35. Accumulators</li> <li>36. Safety injection pumps</li> <li>37. Flow elements Orifices</li> </ol>

Material	Intended Function	Intended Subcomponent
		38. Residual heat removal pumps 39. Residual exchanger tubes (outside/inside) 40. Residual exchanger tube sheets 41. Check valve 42. Heater Sheaths 43. NaOH Storage tank 44. Hydrazine storage tank 45. Eductors 46. Boric acid makeup tank 47. Charging pumps 48. Instrument air system piping/tubing/valves
	Fission Product Barrier (FPB)	1. Penetrations 2. Containment Isolation Valves 3. Containment Penetrations 4. Reinforced Concrete 5. Steel Bellows 6. Structural Steel
	Debris Protector (DP)	1. Strainers
	Heat Transfer (HT)	1. Excess letdown Heat Exchanger tubes 2. Regenerative heat exchangers 3. Thermal Barrier heat exchanger tubes 4. Exchanger nozzles 5. Containment tube coil bands and clips 6. Residual exchanger tubes (outside/inside)
	Support Thimble Tubes	1. Instrumentation tube/tube safe ends 2. Bottom mount Instrumentation guide tubes 3. Seal table fittings 4. Seal tables
	Flow Distribution	1. Lower core plates and fuel pins 2. Core barrels and flanges 3. Baffle and former assemblies 4. Head cooling spray nozzles 5. Lower support castings 6. Containment cyclone separators 7. Flow elements

<b>Material</b>	<b>Intended Function</b>	<b>Intended Subcomponent</b>
	Core Support	<ol style="list-style-type: none"> <li>1. Lower core plates and fuel pins</li> <li>2. Core barrels and flanges</li> <li>3. Lower support columns</li> <li>4. Radial keys and clevis inserts</li> <li>5. Baffle and former assemblies</li> <li>6. Upper support plates/columns</li> <li>7. Head/vessel alignment pins</li> <li>8. Guide tubes/pins</li> <li>9. Internals hold-down springs</li> <li>10. Bottom mounted Instrumentation column</li> <li>11. Upper Instrumentation column</li> <li>12. Lower support castings</li> <li>13. Bolting upper/lower support column</li> <li>14. Bolting guide tube</li> <li>15. Bolting clevis insert</li> <li>16. Bolting baffle/former</li> <li>17. Bolting barrel/former</li> </ol>
	Filtration	<ol style="list-style-type: none"> <li>1. Debris screen banding</li> </ol>
Copper Alloy	Pressure Boundary (PB)	<ol style="list-style-type: none"> <li>1. Fittings</li> <li>2. Heat Exchangers</li> <li>3. Tubing</li> <li>4. Valves</li> <li>5. Cooling Unit tubes/fittings</li> </ol>
	Heat Transfer (HT)	<ol style="list-style-type: none"> <li>1. Heat Exchangers</li> </ol>
Aluminum Alloy	Pressure Boundary (PB) Structural Support (SS)	<ol style="list-style-type: none"> <li>1. Ductwork</li> <li>2. Heat Exchangers</li> <li>3. Instrument air system piping/tubing/valves</li> <li>4. Motor Bearing cooler fins</li> </ol>
	Heat Transfer (HT)	<ol style="list-style-type: none"> <li>1. Heat Exchangers</li> </ol>
	Structural Support (SS)	<ol style="list-style-type: none"> <li>1. Cable trays and supports</li> <li>2. Seismic Restraints for spent fuel storage</li> <li>3. Cover plates – Pull boxes</li> </ol>
Elastomers & Zinc Alloy	Pressure Boundary (PB) Structural Support (SS)	<ol style="list-style-type: none"> <li>1. Ductwork</li> <li>2. Panel Joint seals and sealant</li> </ol>
Concrete	Structural Support (SS) Flood Barrier Radiation Shielding (RS) Missile Barrier (MB) Fission Product Barrier (FPB) Heat Sink	<ol style="list-style-type: none"> <li>1. Reinforced Concrete</li> <li>2. Retaining walls</li> <li>3. Caissons</li> <li>4. Service Water Intake Structures (SWIS)</li> </ol>
Galvanized Steel	Structural Support (SS)	<ol style="list-style-type: none"> <li>1. Anchors/Bolts</li> <li>2. Miscellaneous Steel</li> <li>3. Hangers/Supports for ASME Class I Piping</li> <li>4. Cable trays and supports</li> </ol>

<b>Material</b>	<b>Intended Function</b>	<b>Intended Subcomponent</b>
	Radiation Shielding (RS) Pipe Whip Restraint	1. Miscellaneous Steel
Glass	Pressure Boundary (PB)	1. Fittings 2. Sight glass
Low-Alloy Steel with Stainless Steel Cladding	Pressure Boundary (PB)	1. Closure head domes/flanges 2. Primary inlet/outlet nozzles 3. Intermediate Shells 4. Lower shells 5. Circumferential welds 6. Bottom head toruses/domes 7. Tube sheets
Carbon Steel with Stainless Steel Cladding	Pressure Boundary (PB)	1. Upper and lower heads 2. Surge/Spray/Safety/Relief nozzle 3. Manway covers 4. Channel heads 5. Primary inlet/outlet nozzles 6. Inlet/outlet safe ends 7. Primary manways
Alloy Steel	Pressure Boundary (PB)	1. Upper/lower shells 2. Elliptical heads 3. Transition cones 4. Feedwater nozzles 5. Steam outlet nozzles 6. Blowdown nozzles 7. Seismic lugs 8. Shells 9. Tube sheets 10. Conical skirt 11. Closure bolting
	Throttle	1. Steam flow limiters
Alloy 600	Pressure Boundary (PB)	1. Control Rod drive mechanism house tubes 2. Head vent pipes 3. Core support lugs 4. Instrumentation tube/tube safe ends 5. U-tubes 6. Heater sleeves 7. Nuclear Sampling cooling tubes
	Core Support	1. Radial keys and clevis inserts
	Flow Distribution	1. Divider Plates
Alloy 690 TT	Pressure Boundary (PB)	1. Steam generator tube plugs 2. Heater sleeves 3. Tube plugs
Alloy X-750	Core Support	1. Bolting upper/lower support column 2. Bolting guide tube 3. Bolting clevis insert

<b>Material</b>	<b>Intended Function</b>	<b>Intended Subcomponent</b>
Chrome-plate Alloy 600	Structural Support (SS)	1. Anti-vibration bars
Admiralty Brass	Pressure Boundary (PB)	1. Emergency containment cooler tubes 2. Reactor cooling coils 3. Instrument air system piping/tubing/valves
	Heat Transfer (HT)	1. Emergency containment cooler tubes
Cast Iron	Pressure Boundary (PB)	1. Containment spray pump seal water heat exchanger shells and covers 2. Safety injection pump thrust bearing coolers 3. Injection pump shells and covers 4. Safety bearing coolers 5. Instrument air system piping/tubing/valves 6. Filters/Strainers
Brass	Pressure Boundary (PB)	7. Containment spray pump seal water heat exchanger tub shields 8. Containment exchanger flex fittings 9. Safety injection pump shaft seal heat exchanger tube shields 10. Emergency floodjet spray nozzles 11. Containment cooler flex connectors 12. Cooling Unit tubes/fittings 13. Dampeners 14. Filters/Strainers
Bronze	Pressure Boundary (PB)	1. Spray nozzles
Inconel	Pressure Boundary (PB) Heat Transfer (HT)	1. Safety injection pump shaft seal heat exchanger tubes (inside) 2. Safety injection pump shaft seal heat exchanger tubes (outside)
Rubber	Pressure Boundary (PB)	1. Flexible hose and coupling

Table 2-2 Dominant Materials for Selected Components

Component Category	Materials	Environments	Aging Effects Requiring Management
Exchangers	Alloy 600 Alloy 690 Alloy Steel Alloy X-750 Aluminum Brass Bronze Carbon Steel Carbon Steel w/ SS Cladding Cast Iron Chrome-plated Alloy 600 Copper Copper Alloy Copper Nickel Gray Cast Iron Low Alloy Steel Nickel-Based Alloy Stainless Steel	Air (Ext) Air (Int) Containment Air(Ext) Gas (Ext) Gas (Int) Lubricating Oil (Int) Oil (Ext) Oil (Int) Plant Indoor Air (Ext) Raw Water (Ext) Raw Water (Int) Steam (Int) Treated Water (Ext) Treated Water (Int)	Buildup of Deposit Crack initiation and growth Cracking Heat transfer degradation Loss of Material Loss of Material – Erosion Loss of Material – Selective Leaching Loss of preload
Piping Systems	Alloy 600 Alloy Steel Bare Copper Brass Brass Alloy Bronze Carbon Steel Cast Iron Copper Alloy Copper Nickel Galvanized Steel	Air (Int) Atmosphere/Weather (Ext) Concrete (Ext) Containment Air (ext) Gas (Int) Oil (Int) Plant Indoor Air (Ext) Primary containment Air (Ext) Raw Water (Ext) Raw Water (Int) Soil (Ext)	Buildup of Deposit Cracking Heat transfer degradation Loss of Material Loss of Material – Erosion Loss of Material – Fretting Loss of Material – Selective Leaching

Component Category	Materials	Environments	Aging Effects Requiring Management
	Gray Cast Iron Low Alloy Steel PVC Rubber Stainless Steel	Steam (Ext) Steam (Int) Treated Water (Int) Wet Air/Gas (Int)	
Reactor Pressure Vessel (RPV)	Alloy 600 Alloy X-750 Carbon Steel Cast Austenitic Stainless Steel Copper Alloy Low Alloy Steel Nickel-Based Alloy Stainless Steel Steel Alloys	Containment Air (Ext) High prity water Primary Containment Air (Ext) Reactor coolant water Steam (Int) Treated Water (Ext) Treated Water (Int)	Changes in dimensions Crack initiation and growth Cracking Cumulative Fatigue Loss of Material Loss of preload Reduction in fracture toughness
Tanks	Aluminum Carbon Steel Carbon Steel w/ SS Cladding Cast Austenitic SS Epoxy Coated Carbon Steel Fiberglass PVC Stainless Steel	Air (Int) Air/Gas (Int) Atmosphere/Weather (Ext) Containment Air (Ext) Fuel Oil (Int) Lubricating Oil (Int) Plant Indoor Air (Ext) Primary Containment Air (Ext) Raw Water (Int) Soil (Ext) Treated water (Int) Wet Air/Gas (Int)	Cracking Loss of Material
Concrete	Concrete Concrete Block Grout	Air/Gas Atmosphere/Weather (Ext) Containment Air (Ext) Plant Indoor Air (Ext)	Aggressive chemical attack Change in Material Properties Corrosion of embedded steel Cracking

Component Category	Materials	Environments	Aging Effects Requiring Management
		Raw Water (Ext) Soil (Ext)	Cracking / Loss of Bond/Material Cracking and Expansion Increase in porosity and permeability Leaching of calcium hydroxide Loss of Material Loss of Strength Reduction in Concrete Anchor Capacity
Structural Steel and other Metals	Aluminum Bronze Carbon Steel Cast Iron Galvanized Stainless Steel	Air/Gas Atmosphere/Weather (Ext) Containment Air (Ext) Plant Indoor Air (Ext) Raw Water (Ext) Treated Water (Ext)	Cracking Loss of Leak Tightness Loss of Material Loss of Mechanical Function

Note:

Loss of Material: Crevice Corrosion, FAC, Galvanic Corrosion, General Corrosion, MIC, Pitting Corrosion  
Steel Alloys: Various SA 182, SA 336, SA 350, SA 508, SA 516, etc.

Degradation Occurences by Components

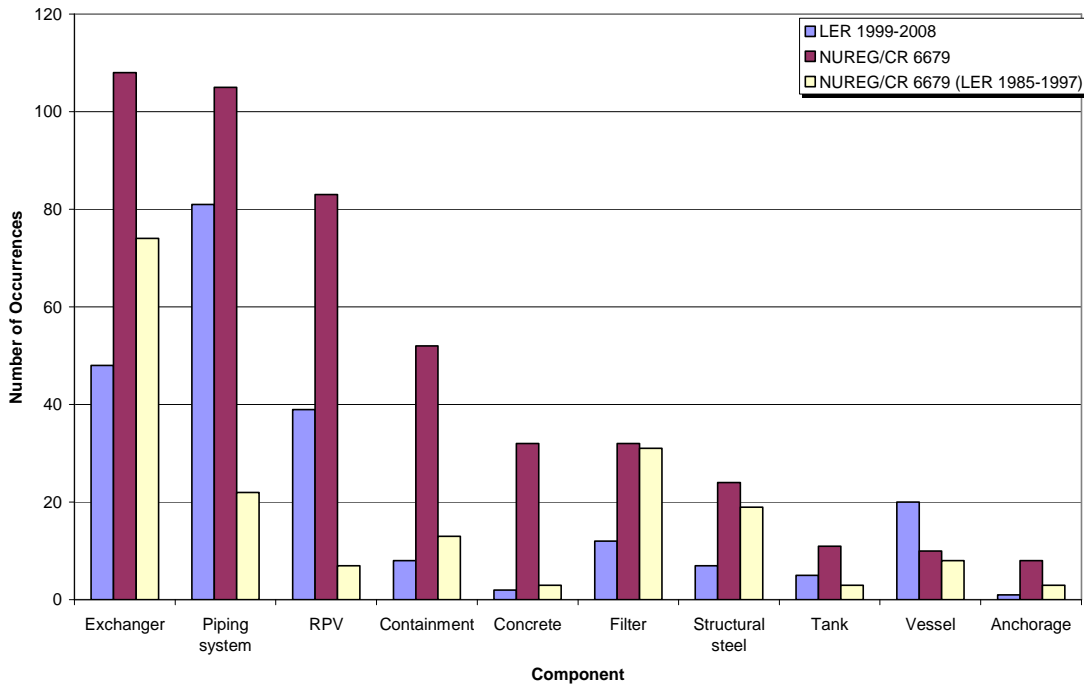


Figure 2-1 Distribution Comparison of SPC Degradation Occurrences over Component

Normalized Occurences

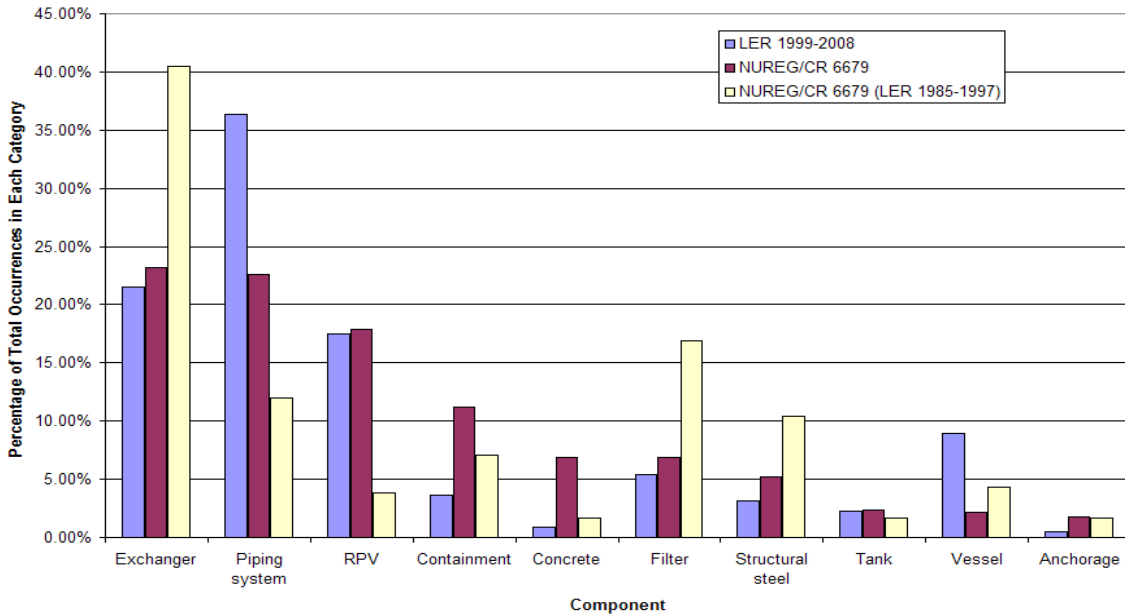


Figure 2-2 Comparison of Normalized Distribution of SPC Degradation Occurrences over Component



### 3 DEGRADATION MODELS FOR CONCRETE

Concrete as the most common construction material for NPPs has been under active research for degradation, especially because degradation of structures and passive components (SPCs) has been a critical consideration when the operating licenses of NPPs are extended beyond their initial operating license period. The importance of the aging-related degradation of concrete components and structures lies in that they are in general used to house the reactors and other importance equipment, guard their safety against large natural disasters such as earthquakes, and contain and mitigate the postulated release of radioactive materials. A recent study [Naus, 2007] indicated, using data from a survey of the U.S. utilities, that the design and construction errors were the major contributors to the problems associated with concrete in NPPs and these problems were corrected when they initiated during construction. This assures that the concrete construction in NPPs is of high quality in material selection, batching, mixing, placing, curing, and other construction processes. However, prolonged exposure of the concrete structures and components to harsh environments, such as freezing and thawing, elevated temperature, irradiation, vibration/fatigue, chemical attacks, etc., can lead to degraded material/component properties. The same report also recognizes that although most of the concrete structures and components in NPPs can meet their performance expectation during the current (40 years) and extended (20 years) operating license period, isolated degraded concrete members may not always be able to meet the desired performance expectation without appropriate maintenance. In fact, degradation of SPCs, especially concrete SPCs, were observed and found to be in need of maintenance by the licensees when NRC staff conducted on-site audits of six plants between July 1991 and August 1992 [NUREG-1522, 1995]. The difficulty in maintenance programs for concrete structures in the past was due in part to lack of accessibility for identification of degradation occurring within the concrete members and the belief that concrete structures were originally built to be highly reliable.

With a substantial list of references, Naus [2007] provides an extensive and in-depth review of important factors that contribute to concrete degradation, with emphasis on factors that apply in NPP environment. Degradation of concrete members can occur in the concrete material, reinforcing steel, prestressing steel, and/or liner steel. For these material types, this reference has a detailed table for degradation factors that can impact the performance of concrete members, which includes categories such as aging stressors/service conditions, aging mechanism, aging effect, potential degradation site, and relevant notes. As described in this report, water is the single most important factor controlling the degradation process of concrete. Other primary factors, that may not applicable for all concrete members, include freezing and thawing, aggressive chemical attacks, abrasion, corrosion of steel reinforcement and other embedded metals, and chemical reactions of aggregates. Cracking is the most dominant degradation effect for concrete, and can lead to reinforcement corrosion. Primary concerns of aging related degradation in concrete members relate to corrosion of steel reinforcement and liner, leaching, and loss of adequate pre-stress.

Given the composite nature of reinforced concrete material, the many factors that contribute to concrete degradation, and the complexity of the physical processes in concrete degradation, it is impossible to have a universal model that encapsulate all these parameters. Similarly, the effort in locating models that cover all related factors can be tremendous, if these models exist at all. Therefore, the effort will be concentrated on the available information for viable models that are potentially important in the fragility analysis.

In Section 3.1 which follows, an overview of cracking in terms of the relationship between crack characteristics and corrosion is given. In Sections 3.2 through 3.6, a description of several time-

dependent degradation models for concrete and steel reinforcement (rebars) is presented. It should be noted that this description provides a summary of the degradation models and presents the fundamental equations along with the key parameters used to define the degradation. For further information and proper implementation of these models, the references cited should be utilized. For the convenience of notation, some models are designated as the name of the leading author that the referenced model was reviewed, but not necessarily as the first person who developed the model.

### **3.1 Overview of Cracking and Corrosion**

Appendix C of the report by Naus [2007] provides some discussion on concrete cracking and steel reinforcement corrosion based on research findings from 36 different sources. The discussion is grouped into two aspects: (1) how crack characteristics affect corrosion, and (2) how corrosion affects crack characteristics.

#### **3.1.1 Effects of Crack Characteristics on Corrosion**

As reported, experiments have not shown a definitive conclusion for the influence of the cracks on the corrosion of steel reinforcement. Depending on the crack orientation, either in parallel with the reinforcement or intersecting the reinforcement, the effects of crack characteristics on corrosion of steel reinforcement can be different. Some researchers believe that cracks create passages for corrosion agents such as carbon dioxide, chlorides, water, and oxygen to reach the reinforcement and provide storage space for corrosion products, therefore accelerate corrosion initiation. Many concrete codes accept this theory by limiting the crack widths at the concrete surface based on surrounding environments. This theory was confirmed by experimental results [e.g., Ida and Yokomuro, 1987]. Some other researchers believe that although cracks in concrete may accelerate corrosion initiation, continuing corrosion is minimal because corrosion is confined to the vicinity of crack-rebar intersections.

For cracks that intersects with steel reinforcement, it has been assumed that the localized corrosion occur only at a zone of 3 times of the rebar diameter around the crack. However, recent studies showed that the corrosion zone could be 13 times as long as the rebar diameter. There was evidence that the width of surface cracks may relate to the length of corroded rebar but not to the amount (depth) of corrosion [Beeby, 1979], as shown by Table 3-1 in which the specimens with various crack widths were stored outdoors for 10 years. It is also reported that test data showed a linear relationship between the degree of corrosion and the surface crack width for exposures of 1 and 2 years, but this relationship did not hold for exposure periods extending to 4 and 10 years. This conclusion coincides with the theories discussed in the previous paragraph, i.e., the crack width affects the corrosion initiating time but not significantly thereafter. A reported recent study by Francois and Arliguie [1999] showed that corrosion of rebars was not significantly affected by cracks with widths up to 0.5 mm, however was influenced by loading. Little evidence has been found showing wider cracks lead to faster corrosion of rebars [Beeby, 1978]. In summary, larger crack widths are likely to start corrosion earlier but the rate of corrosion are not significantly influenced by crack widths.

It is also reported that the time-dependent behavior of the cracks can have different effects on corrosion. Cracks with unvarying widths may be blocked or self-healed by deposition and therefore do not cause further corrosion after corrosion initiation. On the other hand, active cracks, such as those caused by varying loads, can provide the corrosion agents the access to the steel reinforcement. The frequency or the number of cracks also has an influence on corrosion depth. Surface cracks are not always accurate indicators of possible corrosions because their widths may vary through the cover or they may not reach the steel reinforcement.

### 3.1.2 Effects of Corrosion on Crack Characteristics

The second aspect of the relation of cracks and corrosion is that corrosion of steel reinforcement can result in concrete cracking. Cracking due to corrosion of reinforcing steel is important because cracking of concrete cover accelerates corrosion and consequently completes a positive feedback loop. Based on studies of the deterioration of bridge decks, concrete cracking occurs in 2 to 5 years after corrosion initiation [Cady and Weyers, 1984], a time range designated as cracking period. Corrosion rate has been found to be the most important factor in determining the cracking period, while the concrete cover depth, rebar configuration, and concrete grade are not as significant. Table 3-2 shows the relation between the time for visible cracks and the various levels of corrosion rate found in field conditions [Andrade, Alonso, and Molna, 1993]. The ratio of cover to rebar diameter ( $C/d$ ) is a significant corrosion protection parameter. For  $C/d > 2$ , rebar radius losses of 50  $\mu\text{m}$ , 100-200  $\mu\text{m}$ , and 300  $\mu\text{m}$  result in crack widths of about 0.05 mm, 0.3 mm, and 1 mm, respectively. For  $C/d \leq 2$ , a crack width of 0.05 mm only requires a rebar radius loss of 15-30  $\mu\text{m}$  [Alonso, et al., 1998]. Definite conclusions for larger crack width cannot be drawn because of large data scattering. After crack initiation, linear relationship can be sought between crack width and rebar radius loss up to 200 to 300  $\mu\text{m}$ ; above this level of radius loss, such a relation cannot be prescribed because the configuration of structural elements dominate.

General conclusions on cracking of concrete cover and corrosion of rebars are provided by Naus [2007]. These general conclusions, as guidelines, are also important in the selection of degradation models for concrete SPCs. These general conclusions are quoted in the following.

- Crack characteristics of importance to corrosion include width, orientation, or type; propagation status; frequency of occurrence; and shape;
- Although larger crack widths increase the probability of corrosion, values of crack width are not always reliable indicators of corrosion or deterioration expected;
- There appears to be a relationship between surface crack width and corroded length, but it is difficult to define a relationship between surface crack width and magnitude of corrosion;
- Cracks along reinforcement are of more importance than transverse cracks relative to accelerating corrosion;
- Active crack widths are more likely to accelerate the corrosion process than passive crack widths;
- Load can accelerate the corrosion process;
- Visible cracks due to corrosion appear after reinforcing section losses of 10 - 50  $\mu\text{m}$ ;
- Ratio of cover to bar diameter is a significant corrosion parameter, with amount of corrosion required to produce cracking increasing as ratio increases;
- Experimental results indicate that performance of beams, columns, and walls exhibiting corrosion can improve up to point of concrete cracking; and
- Corrosion cracking can affect failure mode, with cracks that coincide with loading direction having the most effect.

### 3.2 The Power Model

In a study of reliability-based service life prediction, Mori [2005] assembled a set of models that represent time-dependent concrete strength increase and property deterioration. This set of

models were collected from the literature [Albrecht and Naeemi, 1984; Clifton and Knab, 1989; Tuutti, 1982; Vesikari, 1988; Washa and Wendt, 1975; Washa, et al, 1989]. Their applications are very straight forward because the study by Mori fits the current research agenda that will be focused on fragility in the next phase.

The strength of concrete, if prepared well during construction, can increase due to hydration beyond the initial 28 days when the compressive strength  $f'_c$  is specified. This increase can be as large as 2 times or more if protected from harsh environment. Equation 3-1 shows an experimental equation for the increase of  $f'_c(t)$  derived from experiments over 50 years [Washa and Wendt, 1975; Washa, et al, 1989]. The study showed that the increase of  $f'_c(t)$  has a linear relation with the logarithm of age during the first 10 to 50 years, and changes very little in the time after. The time-dependent compressive strength of concrete,  $f'_c(t)$ , can be expressed as,

$$f'_c(t) / f_{c_{28}} = \begin{cases} \alpha + \beta \ln t & t < t_M \\ \alpha + \beta \ln t_M & t \geq t_M \end{cases} \quad (3-1)$$

where  $f_{c_{28}}$  is the 28-day compressive strength,  $t$  is time in days, and  $t_M$  is the age to maturity. Parameter  $t_M$  depends on the concrete chemical composition. For concrete consisting of relatively low  $C_2S$ ,  $t_M \approx 10$  years and  $f'_c(t_M)/f_{c_{28}} = 1.67$ , which results in  $\alpha = 0.541$  and  $\beta = 0.138$ . The coefficient of variation in the 50-year compressive strength of concrete varies between 5% and 10%, which is relatively low for engineering materials.

As pointed out by Mori [2005], permeability is the most important factor controlling the quality of concrete, because it controls the rate of ingress of aggressive substances. It should be noted that this observation does not contradict with that of Naus's [2007] stating that water is the most important factor in concrete degradation, because water is the major factor affecting the permeability of concrete and degradation occurs mostly when water is present. Mori [2005] also noted that the most significant stressors for concrete strength degradation include freeze-thaw, sulfate attack, alkali-silicate reactions within concrete, and fatigue. It was also pointed out that corrosion is the most important degradation mechanism for deformed rebars, and loss of prestress by tendon relaxation, anchorage failure, or concrete creep is the most important one for prestressing tendons.

The depth of attack or deterioration can often be represented by the following power model,

$$X(t) = \begin{cases} 0 & \text{for } t < T_I \\ C(t - T_I)^\alpha & \text{for } t \geq T_I, \end{cases} \quad (3-2)$$

in which  $t$  is the elapsed time,  $T_I$  the initiation time for the deterioration process,  $C$  the rate parameter that depends on the concrete mix and its environment/loading, and  $\alpha$  the order of the power model that depends on the nature of the attack. Parameters  $C$  and  $\alpha$  must be determined from tests suitable for the concrete component of interest. For diffusion-dominant degradation processes,  $\alpha = 1/2$ , while it can also be greater than one for other degradation mechanisms.

For uniform corrosion of steel reinforcement,  $X(t)$ , which is measured in  $\mu\text{m}$  and in years, the degradation rate parameter  $C$  can be found in the literature to be in a range of 50 to 125 and the parameter  $\alpha$  is in a range of  $1/2$  to 1. The coefficient of variation in  $C$  can be as large as about 0.5; while  $\alpha$  can be treated as deterministic.

Factors affecting the time to initiate corrosion of steel rebars,  $T_I$ , include at least the permeability of concrete, existing surface cracks, and the thickness of concrete cover. Carbonation, a process

that carbon dioxide penetrates the concrete cover and reduces the natural alkalinity of concrete, is a diffusion-dominant process. Corrosion starts when the depth of carbonation or penetration of aggressive ion reaches the steel reinforcement. The depth of carbonation can be modeled as,

$$X(t) = K\sqrt{t}, \quad (3-3)$$

where  $K$  is an experimental constant, and for cases with no exposure to rain, it can be estimated as [Tuutti, 1982],

$$K = 26(W/C - 0.3)^2 + 1.6 \text{ (mm/year}^{1/2}\text{)}, \quad (3-4)$$

in which  $W/C$  is the weight water-cement ratio. Although cracking in concrete do not always represent actual degradation in concrete strength, it can greatly decrease the initiation time  $T_I$ . For these cases where cracks are present, the depth of carbonation can be found using the crack width,  $w$ ,

$$X(t) = 50\sqrt{w} \sqrt[4]{t} \text{ (mm)}. \quad (3-5)$$

The corrosion initiation time  $T_I$  has been assumed log-normally distributed with a coefficient of variation equal to 0.20 [Vesikari, 1988].

For fragility analysis, a limit state can be defined as a function of the structural resistance  $R(t)$  of interest and the relevant loads. For a given limit state, the required structural resistance, such as flexural, shear, or compression strength, can include the depth of attack  $X(t)$  to consider the level of degradation. It should be noted that the structural resistance as a function of the depth of attack may not be linear. As an example, the reduction of the tensile strength of a rebar due to loss of section area from corrosion can be determined by,

$$R(t)/R_0 = \left[ 1 - \frac{2C(t - T_I)^\alpha}{D} \right]^2 \quad (3-6)$$

in which  $R_0$  is the tensile strength of reinforcing bar without corrosion.

### 3.3 Thoft-Christensen's Model

#### 3.3.1 Time for Corrosion Initiation by Chloride Penetration

Corrosion initiation time  $T_I$ , refers to the time during which the passivation of steel reinforcement is damaged and the active corrosion of rebars starts. This process is fairly complex so that an accurate understanding of the underlining physical and chemical processes is not available.

One of the models is based on Fick's law of diffusion to represent the rate of chloride penetration into concrete [Thoft-Christensen, 2003; Li, et al, 2003]. Given  $x$  as the depth from the concrete surface and  $t$  as time, the chloride ion concentration  $C(x, t)$ , as weight percentage of cement, satisfies the following partial differential equation,

$$\frac{\partial C(x, t)}{\partial t} = D_c \frac{\partial^2 C(x, t)}{\partial x^2} \quad (3-7)$$

in which  $D_c$  is the chloride diffusion coefficient with a unit of  $[\text{Length}^2]/[\text{Time}]$ . The solution of Equation 3-7 can be shown to be,

$$C(x, t) = C_0 \left[ 1 - \text{erf}\left(\frac{x}{2\sqrt{D_c \cdot t}}\right) \right], \quad (3-8)$$

in which  $C_0$  is the equilibrium chloride concentration on the concrete surface, and erf is the error function. Models with spatial and time variation of  $C_0$  or variation of  $D_c$  with respect to  $x$  have also been developed in the literature. Inversion of Equation 3-8 can lead to the following equation to determine the corrosion initiation time  $T_I$ ,

$$T_I = \frac{d^2}{4D_c} \left\{ \text{erf}^{-1} \left( \frac{C_0 - C_{cr}}{C_0} \right) \right\}^{-2} \quad (3-9)$$

The diffusion coefficient  $D_c$  is not a physical parameter of a concrete member and therefore must be determined by experiments. Studies in the literature have shown that the most important factors that affect  $D_c$  are the water-cement ratio  $W/C$ , temperature  $\Phi$ , and the amount of e.g., silica fume.  $D_c$  increases significantly as  $W/C$  and/or  $\Phi$  increase. Thoft-Christensen [2003] provided a figure showing  $D_c$  as a function of  $W/C$  and  $\Phi$  for concrete of 0% silica fume. From that figure, the minimum value of  $D_c$  was reported as  $0.31 \times 10^{-12} \text{ m}^2/\text{s}$  for  $W/C=0.2$  and  $\Phi = 4^\circ\text{C}$ , and the maximum value of  $D_c$  as  $80 \times 10^{-12} \text{ m}^2/\text{s}$  for  $W/C=0.70$  and  $\Phi = 35^\circ\text{C}$ .

### 3.3.2 Corrosion of Reinforcement

After the initiation of reinforcement corrosion, the corrosion evolution process can be very complicated. Thoft-Christensen [2003] provided a simple linear relationship for the rebar diameter  $D(t)$  as,

$$D(t) = D_0 - C_c R_c (t - T_I), \quad t \geq T_I, \quad (3-10)$$

in which  $D_0$  is the initial diameter,  $C_c$  a corrosion coefficient, and  $R_c$  the corrosion rate.

### 3.3.3 Initiation of Cracking

Around the interface between the rebars and concrete, there is a porous zone that can accommodate a certain amount of corrosion products. The porous zone is not a homogeneous field with voids, with porosity (*the ratio of the void volume to the total bulk volume*) close to 1 at locations close to the rebars. Let  $H_P$  be the thickness of an equivalent zone around a rebar with porosity 1 and  $\rho_C$  be the density of corrosion products, the amount of corrosion products that the porous zone can accommodate can be expressed as,

$$W_P = H_P \cdot \pi \cdot \rho_C \cdot D_0 \cdot (3-11)$$

Upon filling up the porous zone, the corrosion products start to produce expansive pressure in concrete near the rebars and eventually result in cracks when the corrosion process continues. The corrosion products at initial cracking of concrete occupy the porous zone, the expansion of the concrete ( $W_E$ ), and the space of corroded steel ( $W_S$ ). The total amount of corrosion products that leads to the incipient development of cracks at time  $T_C$  is designated as the critical corrosion products  $W_C$ , which can be expressed as,

$$W_C = W_P + W_E + W_S \cdot (3-12)$$

Let  $H_E$  be the thickness of the expanded concrete around the corroded rebar at time  $T_C$ , then,

$$W_E = H_E \cdot \rho_C \cdot \pi(D + 2H_P) . \quad (3-13)$$

By assuming the concrete homogenous and elastic and using a thick-walled concrete cylinder model, Liu and Weyers [1998] derived the critical expansion thickness  $H_E$  to be,

$$\begin{aligned} a &= (D + 2H_P)/2 \\ b &= c + (D + 2H_P)/2 \\ H_E &= \frac{c f'_t}{E_{ef}} \left( \frac{a^2 + b^2}{b^2 - a^2} + \nu_c \right) , \end{aligned} \quad (3-14)$$

in which  $c$ ,  $E_{ef}$ ,  $f'_t$ ,  $\nu_c$  are the concrete cover, effective elastic modulus, tensile strength, and Poisson's ratio of the concrete, respectively.

The corrosion products that occupy the steel reinforcement space,  $W_S$ , can be determined by,

$$W_S = \frac{\rho_C}{\rho_{steel}} M_{steel} , \quad (3-15)$$

in which  $M_{steel}$  and  $\rho_{steel}$  are the mass of the corroded steel and the density of steel, respectively. It should be noted that  $M_{steel}$  is proportional to  $W_C$ ; the ratio between them have been found to be 0.523 or 0.622 for two types of corrosion products [Liu and Weyers, 1998]. Assuming  $M_{steel} = 0.57W_C$  for simplicity, solving Equation 3-12 yields,

$$W_C = \frac{\rho_{steel}}{\rho_{steel} - 0.57\rho_C} (W_P + W_E) . \quad (3-16)$$

Liu and Weyers [1998] formulated the rate of corrosion production as a function of time (years) starting at corrosion initiation as,

$$\frac{dW_{rust}(t)}{dt} = \frac{k_{rust}(t)}{W_{rust}(t)} . \quad (3-17)$$

In which  $W_{rust}(t)$  is the corrosion products and  $k_{rust}(t)$  can be assumed as,

$$k_{rust}(t) = 0.383 \times 10^{-3} D R_C(t) \quad (3-18)$$

Integrating Equation 3-17 gives,

$$W_{rust}^2(t) = 2 \int_0^t k_{rust}(t) dt \quad (3-19)$$

When the corrosion rate  $R_C(t)$  can be modeled as time-independent, the incremental time  $\Delta t_{crack}$  from corrosion initiation to incipient cracking can be estimated from the above integral by letting  $W_{rust}(\Delta t_{crack})=W_C$ ,

$$\Delta t_{\text{crack}} = \frac{W_c^2}{2k_{\text{rust}}} = \frac{W_c^2}{2 \times 0.383 \times 10^{-3} D R_c} \quad (3-20)$$

The crack initiation time is then given by,

$$T_{\text{crack}} = T_I + \Delta t_{\text{crack}} \cdot \quad (3-21)$$

### 3.3.4 Corrosion Crack Evolution

As corrosion production continues, the crack width will be increasing, starting with an initial crack width  $w_0$  at  $T_{\text{crack}}$ . Field measurements have not yet been possible to establish a time-dependent model for the crack growth. Thoft-Christensen [2003] showed a simple linear relationship between the crack width  $w(t)$  and the decrease of the diameter  $D$  given by,

$$\Delta w = \gamma \Delta D, \quad (3-22)$$

where  $\gamma$  was estimated to be in a range of 1.5 to 5 by Andrade et al. [1993].

Another approximation to the relationship between  $\Delta w$  and  $\Delta D$  was developed by Thoft-Christensen [2003] by assuming that the total crack volume equals the volume of the corrosion products, and is shown by the following equation,

$$\frac{1}{2} \left( \frac{D/2}{D/2 + c} + 1 \right) c \Delta w = \left( \frac{\rho_{\text{rust}}}{\rho_{\text{steel}}} - 1 \right) \pi D \frac{\Delta D}{2}. \quad (3-23)$$

The ratio  $\rho_{\text{rust}}/\rho_{\text{steel}}$  has a value typically in the range of 2 to 4, depending on the type of corrosion products. This model is similar to the linear model as shown in Equation 3-22; an example using this model showed an equivalent  $\gamma$  in the range of 1.4 to 4.2, in good agreement with the test results [Andrade et al., 1993].

Spalling of concrete can be simulated by finite element analysis by combining the models developed above. The criterion for the spalling occurrence is that a set of cracks form a mechanism to separate a piece of concrete from the SPC.

### 3.4 Basheer's Model

Besides a qualitative macro-predictive model developed by Basheer, et al. [1996], a micro predictive model was also formulated for quantitative prediction of the deterioration of concrete structures. This model consists of transport models for the moisture, ions, and heat transfer through the cement paste, deterioration models for the corrosion, physical and chemical processes, and a structural model for the crack development and the associated strength reduction and dimension changes. This model was implemented using the finite element method (FEM). This micro model can be adapted for use in the context of fragility analysis, especially for those fragilities developed using FEM. Only the chloride based model was presented in Basheer, et al. [1996].

### 3.4.1 Transport Model for Chloride Ions

This chloride ion transport model is different from the Thoft-Christensen model [2003], in that the principle of mass conservation was added to the Fick's diffusion law. This model can be expressed as,

$$\frac{\partial C}{\partial t} = \text{div}[D_c \nabla(C)] - \frac{1}{\omega} \frac{\partial S}{\partial t}, \quad (3-24)$$

in which  $C$  is the free chloride concentration in the porous body ( $\text{mol}/\text{cm}^3$ ),  $S$  the bound chloride ions ( $\text{mol}/\text{cm}^3$ ),  $\omega$  the content of water in which diffusion takes place (per unit mass of cement), and  $D_c$  the chloride diffusion coefficient in the pore solution ( $\text{cm}^2/\text{s}$ ). The relationship between the free and bound chloride, representing the diffusion-reaction-equilibration process, is given by,

$$S = C_t - \omega_e C, \quad (3-25)$$

where  $C_t$  is the total chloride ions ( $\text{mol}/\text{cm}^3$ ) and  $\omega_e$  the evaporable water content. For a fully saturated concrete under isothermal conditions, the free and total chloride concentration can be shown to satisfy the following governing differential equations,

$$\begin{aligned} \left(1 + \frac{\alpha}{\omega_e(1 + \beta C)^2}\right) \frac{\partial C}{\partial t} &= \text{div}[D_c t^{(0.6-2.5W/C)} \nabla(C)] \\ \left(1 + \frac{\alpha}{\omega_e(1 + \beta C)^2}\right) \frac{\partial C_t}{\partial t} &= \text{div}[D_c t^{(0.6-2.5W/C)} \nabla(C)] \end{aligned} \quad (3-26)$$

where  $\alpha$  and  $\beta$  are constants.

The application of this model will require more effort in implementing the mathematical models in FEM.

### 3.4.2 Corrosion Model

Tutti's model [1982] for corrosion was adopted by Basheer, et al [1996] to consider only the effect of chloride ions. The original Tutti's model considered the combined effect of chloride ions and carbonation. This corrosion model consists of two phases for initiation of corrosion and propagation of active corrosion. The transition between these two periods occurs when the protective passivating film cannot be repaired sufficiently by hydroxyl ions after being damaged by the chloride ions.

The chloride transport model can be used to determine the corrosion initiation period, at the end of which the total chloride ion concentration exceeds the threshold. The threshold total chloride ion concentration has been reported in the large range of 0.2 to 2.8  $\text{kg}/\text{m}^3$  [Funahashi, 1990]. Assuming a threshold of 0.7  $\text{kg}/\text{m}^3$  (0.02  $\text{mol}/\text{cm}^3$ ) and a surface chloride concentration of 2.8  $\text{kg}/\text{m}^3$ , it requires 25 years for the chloride concentration to exceed the threshold at a depth of 7.5 cm.

A simplistic model was used to represent the increase of the diameter of steel rebars due to the production of hydrated red rust, and is given by the following formula,

$$\Delta D = t_{\text{cor}} \frac{s j_r}{D_0 \rho_{\text{cor}}}, \quad (3-27)$$

in which  $D_0$  is the original diameter,  $t_{cor}$  the duration of steady state corrosion,  $s$  the rebar spacing,  $j_r$  the rate of rust production per unit area, and  $\rho_{cor} = [1/\rho_r - 0.583/\rho_{st}]^{-1}\pi/2 \approx 3.6 \text{ g/cm}^2$ , where  $\rho_r$  and  $\rho_{st}$  are the mass densities of  $\text{Fe}(\text{OH})_3$  and steel. This model was simplified even further to,

$$\Delta D \approx \frac{t}{D}. \quad (3-28)$$

### 3.4.3 Structural Model

Following Goltermann's approach [1994], the contact pressure between the rebar and the cement paste is given by,

$$p = \Delta D G_a K_o$$

$$G_a K_o = E_p / \left[ \left( 1 + \frac{\nu_p}{2} \right) + 1.2 \nu_s \frac{E_p}{E_s} \right] \quad (3-29)$$

in which  $E_p$  and  $E_s$  are the Young's moduli of the paste and the steel, respectively, and  $\nu_p$  and  $\nu_s$  are the Poisson's ratios of the paste and the steel, respectively. A crack is initiated when the contact pressure  $p$  exceeds the fracture strength of the concrete.

### 3.5 Sarveswaran's Model

For use in reliability analysis of deteriorating structures, Sarveswaran and Roberts [1999] proposed a linear corrosion model to represent the loss of cross section area of a rebar. This model is given by the following equation,

$$\Delta A = R_c (t - t_{init})$$

$$R_c = (-mE - c) + U_{cor} \quad (3-30)$$

where  $R_c$  is the corrosion rate,  $m$  and  $c$  are empirical coefficients determined from site test,  $E$  is the measured half-cell potential (mV),  $U_{cor}$  is the model uncertainty associated with the corrosion rate model, and  $t_{init}$  is the time at which the chloride concentration at the rebar surface reaches the threshold for corrosion to develop. There was no direct instruction on how to obtain  $m$  and  $c$ .

A model to determine the delaminated length was also given by Sarveswaran and Roberts [1999], however it is not envisioned to be of interest in fragility analysis for the purpose of this research. The application of these models in the reference was combined with resistance and load models that are problem-specific.

### 3.6 Marsh's Model

In developing a reliability model for use in structural health monitoring of bridge decks, Marsh and Frangopol [2008] presented a chloride ingress model and two corrosion models for loss of sectional area of the steel reinforcement: one for general corrosion and one for pitting corrosion. The electrochemical process behind these corrosion models is the same as those described previously in this report. It was pointed out in this paper that the rate of steel loss can be as significant as more than 1mm/year. The corrosion product iron hydroxide has lower density than metallic iron and therefore the increased volume by the corrosion process creates pressure in the concrete. This pressure causes concrete to crack and if severe enough, to spall; the cracking and spalling of concrete allows more moisture and aggressive ions to access the steel reinforcement.

Spalling can severely damage the strength and integrity of concrete structures [Bertolini et al, 2004].

This model considered the chloride-induced corrosion with the assumption of the chloride ion penetration to be dominated by the diffusion process. The time for corrosion initiation  $T_I$  can be modeled by Equation 3-9, which was obtained by solving the Fick's law when the Thoft-Christensen's model was described previously.

The general corrosion model assumes the corrosion occurs uniformly around a rebar section. The area of a rebar section is given by the following time-dependent formula,

$$A(t) = \frac{\pi(D_0 - 2r_c(t - T_I))^2}{4}, \quad (3-31)$$

in which  $r_c()$  is the instantaneous corrosion rate and  $D_0$  the initial diameter of a rebar. It should be noted that the above equation is slightly different from the original Marsh's model in that  $r_c()$  is measured as the reduction rate of the radius instead of the diameter to be consistent with the rest of the models in this report. It should be also noted that the corrosion rate can be nonlinear with respect to time, although this model is essentially very much similar to Equation 3-10 described in the Thoft-Christensen's model.

The distinguishing feature of Marsh's model lies in its introduction of a pitting corrosion model. Chloride-induced corrosion may often be in the form of pitting corrosion instead of a uniform reduction of rebar section area (also known as *general corrosion*). In addition, given the same corrosion rate, pitting can result in much larger cross-sectional area loss than general corrosion, with a factor in the range of 5 to 10 [Stewart MG, 2004]. Being highly localized, pitting corrosion can have a dramatic penetration rate as high as 1 mm/year [Bertolini, et al, 2004].

Since the greatest reduction in cross-sectional area controls the strength of a rebar with pitting corrosion, the maximum pit depth is used as a key parameter to represent the weakest section. Stewart [2004] developed a pitting model based on a relation between the maximum pit depth and the average pit depth, and this model was adapted by Marsh and Frangopol [2008]. Let  $\bar{r}_c$  be the average instantaneous corrosion rate,  $R$  a time-invariant constant that equals the maximum pit depth over average pit depth ( $P_{\max}/P_{AV}$ ) for a given length of rebar, and  $t$  the time since corrosion initiation (years), then the maximum pit depth can be expressed as,

$$p(t) = \bar{r}_c R t. \quad (3-32)$$

Given a rebar with an initial diameter of  $D_0$  (mm), the width  $a$  of the pit and the cross-sectional area  $A_{\text{pit}}$  of the pit can be approximated by the following time-dependent equations [Stewart MG, 2004],

$$a = 2p(t) \sqrt{1 - \left(\frac{p(t)}{D_0}\right)^2}, \quad (3-33)$$

$$A_{\text{pit}}(t) = \begin{cases} A_1 + A_2, & \text{for } p \leq \frac{D_0}{\sqrt{2}}, \\ \frac{\pi D_0^2}{4} - A_1 + A_2, & \text{for } \frac{D_0}{\sqrt{2}} < p(t) \leq D_0, \\ \frac{\pi D_0^2}{4}, & \text{for } p(t) > D_0, \end{cases} \quad (3-34)$$

in which,

$$A_1 = 0.5 \left[ \theta_1 \left( \frac{D_0}{2} \right)^2 - a \left| \frac{D_0}{2} - \frac{p(t)^2}{D_0} \right| \right], \quad (3-35)$$

$$A_2 = 0.5 \left[ \theta_2 p(t)^2 - a \frac{p(t)^2}{D_0} \right], \quad (3-36)$$

$$\theta_1 = 2 \arcsin \left( \frac{a}{D_0} \right) \text{ and } \theta_2 = 2 \arcsin \left( \frac{a}{2p(t)} \right). \quad (3-37)$$

With the cross-sectional area of the pit  $A_{\text{pit}}$ , one can easily apply it to the structural model by reducing the rebar section area.

Table 3-1 Relationship between Surface Crack Width and Corrosion Depth/Length [Beeby, 1979]

Surface crack width (mm)	Average depth of corrosion (mm)	Average corroded length (mm)
0.13	0.16	9.2
0.25	0.16	12.9
0.51	0.18	12.8
1.27	0.21	15.0

Table 3-2 Time to Develop Visible Crack in Concrete Cover vs Corrosion Rate [Andrade, Alonso, and Molina, 1993]

Corrosion Rate (/year)	Time Period (years)	
	Crack Width of 0.05-0.10 mm (Loss of Rebar Cross Area: 20 $\mu\text{m}$ )	Crack Width of 0.2-0.3 mm (Loss of rebar cross section: 100-150 $\mu\text{m}$ )
1 $\mu\text{m}$	20	>100
10 $\mu\text{m}$	2	10-15
1000 $\mu\text{m}$	0.2	1-2
20 mm	0.02	0.1-0.2



## 4 DEGRADATION MODELS FOR CARBON AND LOW-ALLOY STEELS

Carbon and low-alloy steels can be vulnerable to corrosion and fatigue. Several models have been identified to represent these common degradation mechanisms. The first one is the power model for steel corrosion which was described in the previous section and applicable to various environments. The second model is for the dry oxidation for steel subjected to relatively high temperature. Models have been found to represent the fatigue crack growth phenomena in the sense of both deterministic and stochastic; and corrosion fatigue is considered with a corrosion modified fatigue crack growth model. Also identified is a very flexible and powerful corrosion model that can be reduced to various other simpler models.

Sections 4.1 through 4.5 provide descriptions of several time-dependent degradation models for carbon and low-alloy steels. It should be noted that these descriptions provide a summary of the degradation models and present the fundamental equations along with the key parameters used to define the degradation. For further information and proper implementation of these models, the references cited should be utilized. In some cases, these models contain formulations that are partially similar to others, suggesting families of these models exist. For the convenience of notation, some models are designated as the name of the leading author that the referenced model was reviewed, but not necessarily as the first person who developed the model.

### 4.1 The Power Model

The power model used in concrete, as shown by Equation 3-1, can also be used for steel SPCs. The corrosion rate  $C$  is a function of ambient moisture and temperature. The parameters  $C$  and  $\alpha$  can be estimated using experiments. Table 4-1 shows the average values for these parameters determined by Albrecht and Naeemi [1984]. The level of attack  $X(t)$  applicable to this table is in units of  $\mu\text{m}$  as a function of years  $t$ . The NPP environment for the application of these parameters should be evaluated in order to pick the most suitable environment in the table.

### 4.2 Henshall's Model (Dry Oxidation)

Oxidation of metals at constant temperature can be explained by various physical theories. Available experimental data show that dry oxidation of iron and low-carbon steels at moderately elevated temperature ( $293 < T \leq 843\text{K}$ ) is diffusion controlled and therefore the oxide thickness follows a parabolic law when the temperature is constant. For the temperature of interest for this method to be applicable,  $Fe_3O_4$  (magnetite) is (reasonably) assumed to be the only corrosion product, leaving out the thermodynamically unstable  $FeO$  (wüstite) and the less substantial  $Fe_2O_3$  (hematite). In addition, the following assumptions were also made by Henshall [1996] when developing this model:

1.  $Fe_3O_4$  oxide was assumed to be 100% dense based on observations for layers up to 20  $\mu\text{m}$  thick,
2. Arrhenius behavior with a constant activation energy over relevant temperature range was assumed (see Eq. 4-2),
3. Oxidation occurs uniformly across the metal surface,
4. The oxide was assumed to be adherent to the metal surface.

The parabolic relation of the thickness of  $Fe_3O_4$  to the exposure time can be expressed as,

$$\frac{dx}{dt} = \frac{k'_p}{x}, \quad (4-1)$$

in which  $x$  is the thickness of  $Fe_3O_4$ ,  $t$  the exposure time, and  $k'_p$  the parabolic oxidation rate constant. The oxidation rate is temperature dependent and such dependence is modeled by the Arrhenius behavior of  $k'_p$ ,

$$k'_p = k_p \exp\left(-\frac{Q}{RT}\right), \quad (4-2)$$

in which  $k_p$  is a constant,  $Q$  the activation energy for the oxidation process,  $R$  the gas constant ( $8.314472 \text{ J} \cdot \text{K}^{-1} \cdot \text{mol}^{-1}$ ), and  $T$  the absolute temperature (K). In the literature,  $k_p$  varies considerably and a conservative value  $4.3 \times 10^{-5} \text{ cm}^2/\text{s}$  was used by Henshall [1996] as this value is the largest found in the literature. It was also reported that  $Q$  appeared to be constant at about 104 kJ/mol in the parabolic regime and at relatively low temperatures in a range of 523 to 736 K. Lower values of  $Q$  have been reported for higher temperatures. For lower temperatures (323-533 K),  $Q$  was believed to change insignificantly. More details on  $k_p$  and  $Q$  were provided by Henshall [1996].

For simple temperature histories, e.g. constant temperature, the above two equations can be conveniently integrated to determine the thickness of oxide. However, for arbitrary thermal histories, a numerical approach must be resorted to obtain the approximated values. For example, a Forward Euler method can be employed to solve for the increase of the oxide thickness,  $\Delta x$ ,

$$\Delta x = \frac{1}{x} k_p \exp\left(-\frac{Q}{RT}\right) \Delta t, \quad (4-3)$$

where  $\Delta t$  is the time increment. This finite difference equation can be solved to determine the thickness  $x$ .

The thickness of oxide does not directly relate to structural strength, which instead requires the metal penetration by oxidation. The fully dense assumption of  $Fe_3O_4$  leads to the following equation to calculate the metal penetration,  $p$ ,

$$p = \frac{\rho_0}{M_0} \frac{M_M}{\rho_M} N_M x \quad (4-4)$$

in which  $\rho_0$  and  $\rho_M$  are the densities of oxide and metal,  $M_0$  and  $M_M$  the molecular weight of the oxide and the atomic weight of the metal,  $N_M$  the number of metal atoms per molecule of oxide (3 for  $Fe_3O_4$ ).

The stress in the oxide increases as the thickness of the oxide increases and the layer of oxide can crack and spall when a critical thickness  $x_c$  is reached. A conservative estimate of the accumulated penetration  $P$  can be computed by assuming that the oxide completely spalls away at  $x_c$ ,

$$P = \sum_{i=1}^n p_i, \quad (4-5)$$

where  $n$  is the total number of spall events. The critical thickness  $x_c$  was chosen as 0.02 mm or 0.1 mm in the numerical study by Henshall [1996].

### 4.3 Fatigue Crack Growth Models

For high cycle fatigue, the Paris-Erdogan relationship expresses the instantaneous crack growth  $da/dN$  in terms of the cyclical component  $\Delta K$  of the stress intensity factor  $K$  as follows,

$$\begin{aligned}\frac{da}{dN} &= C(\Delta K)^m \\ \Delta K &= Y \delta \sigma \sqrt{\pi a},\end{aligned}\tag{4-6}$$

in which the experimental constants  $C$  and  $m$  are  $2.4 \times 10^{-10}$  and 3, respectively, for mild carbon steels [Barsom and Rolfe, 1987, McAllister and Ellingwood, 2001],  $\Delta \sigma$  the range of the far-field stress,  $Y$  a stress magnification factor, which is a function of crack and geometry and should be determined specifically for a given problem. The cycle-dependent crack size  $a(N)$  can be determined by integrating Eq. 4-6.

Fatigue cracks have considerable variability, arising from stochastic nature of material properties, geometry, surface quality and other internal defects, residual stresses, environment, and loadings. Even with a constant stress range, experimental data of fatigue cracks shows substantial scattering. Therefore, fatigue crack growth should be better modeled as a stochastic process. In light of this uncertainty, the Paris-Erdogan relationship should be considered as a median equation. In the context of time-dependent fragility analysis, if the fragility analyses are performed with various levels of degradation but independent of time, the uncertainty in the degradation models (e.g., fatigue crack growth models in this section) adds another dimension when the time factor is included in the development of acceptance criteria.

The Paris-Erdogan relationship in Eq. 4-6 can be improved to consider the stochastic nature of the fatigue crack growth phenomena, by the following equation,

$$\frac{da}{dN} = C(\Delta K)^m X(N),\tag{4-7}$$

in which  $X(N)$  is a stationary random process with a median of unity, while  $C$ ,  $\Delta K$ , and  $m$  take their median values [McAllister and Ellingwood, 2001]. It has been demonstrated that a lognormal probability density function (PDF) can best fit test data [Virkler et al, 1978]. Building on the assumption of a lognormal stationary random process with a median value of 1.0, Yang and Manning [1996] recently developed a simple autocovariance function that permits a closed form solution for the crack exceedance probability, which is an exponentially decaying function,

$$COV(X(N), X(N + \Delta N)) = \sigma_x^2 \exp(-\zeta_x |\Delta N|),\tag{4-8}$$

in which  $\sigma_x$  is the standard deviation of  $X(N)$  and  $\zeta_x$  a correlation scale parameter. Experimental data showed that  $\sigma_x$  is about 0.3 for mild carbon steel under constant-amplitude stress cycles [Barsom and Rolfe, 1987].  $\zeta_x$  has been assumed to be  $2.5 \times 10^{-6}$ /cycle for mild steel [Zheng and Ellingwood, 1998] and  $1.0 \times 10^{-5}$ /cycle for aluminum [Spencer et al, 1989], partly because aluminum has a larger grain size than mild steel and accordingly a larger correlation factor would be expected. McAllister and Ellingwood [2001] provided a detailed discussion on the determination of  $\sigma_x$  utilizing experimental data.

Using Eqs. 4-7 and 4-8, Yang and Manning [1996] determined a closed form solution for the distribution of the number cycles  $n$  to reach a given crack depth  $a$  (designated as a random variable  $N(a)$ ):

$$F_{N(a)} = \Phi \left[ \frac{\ln n - \ln \left( \frac{n_m(a)}{\lambda} \right)}{\sigma_Z(n)} \right], \quad (4-9)$$

in which  $n_m(a)$  is the median number of cycles to reach a crack depth of  $a$  and  $Z(N)$  is a resulting stochastic process from integrating  $X(N)$ . The factor  $\lambda$  and the standard deviation  $\sigma_Z$  (of  $Z(N)$ ) can be determined using parameters  $\sigma_x$  and  $\zeta_x$ ,

$$\begin{aligned} \sigma_Z(n) &= \sqrt{\ln(1 + \phi^2 \exp(\sigma_x^2) - \phi^2)} \\ \lambda &= \exp\left(\frac{\sigma_Z^2}{2}\right) [1 + \phi^2 \exp(\sigma_Z^2) - \phi^2]^{-1/2} \end{aligned} \quad (4-10)$$

in which  $\phi = \sqrt{2(\exp(-\zeta_x n) + \zeta_x n - 1)}/\zeta_x n$ .

It should be noted that there are some other models for fatigue crack growth, which may be more complex [e.g., McDowell, 1996]

For use in the time-dependent fragility analysis, the cycle number  $n$  can be directly related to service time  $T$  given the loading time history.

#### 4.4 Corrosion-Modified Fatigue Crack Growth Models

An aggressive environment can greatly decrease the fatigue limit stress of a specimen, and so the fatigue process affected by the corrosive environment is specially termed as the corrosion fatigue process. Akid and Miller [1991] concluded that significant reduction in fatigue life due to corrosion arises from the loss of the ability of microstructural features of the specimen to decelerate or stop cracks in the corrosive environment. They also noticed that a transition from environmental controlled crack growth to relatively stress controlled crack growth as crack length increases. The corrosion-modified fatigue crack growth model incorporates the discontinuous growth of a crack arising from inherent barriers in the microstructure, such as grain or phase boundaries. Two models were cited by Akid and Miller [1991].

The first model was derived by Hobson et al. [1986]. The fatigue crack growth is separated into two phases: up to and beyond the major microstructural barrier. This model was derived based on experimental data and can be described by the following two equations,

$$\begin{aligned} \frac{da}{dN} &= A\Delta\gamma^\alpha(d - a) \\ \frac{da}{dN} &= B\Delta\gamma^\beta(a - D), \end{aligned} \quad (4-11)$$

in which  $d$  is the distance between the strongest barriers to crack growth in a given material and  $\Delta\gamma$  the shear strain range (note: the tests were done under fully reversed torsional fatigue loading conditions),  $D$  a stress-dependent threshold value of crack growth rate, and  $A$ ,  $B$ ,  $\alpha$ , and  $\beta$  are material dependent constants.

The second model was developed by Navarro and de los Rios [1988], which is based on a theory of continuously distributed dislocations. This model is expressed as,

$$\begin{aligned}\frac{da}{dN} &= f\phi \\ \phi &= \frac{2(1-\nu)\sqrt{1-n^2}}{G} \sigma a,\end{aligned}\tag{4-12}$$

in which  $f$  is a factor related to the number of dislocations on the active slip band,  $\phi$  a measure of the plastic displacement at the crack tip,  $n$  the ratio of the crack length to plastic zone size,  $G$  the shear modulus, and  $\nu$  Poisson's ratio.

Eqs. 4-11 and 4-12 can be modified slightly to incorporate a term representing the corrosion process of metal dissolution as follows,

$$\frac{da_{cf}}{dN} = \frac{da_{air}}{dN} + \frac{da_{diss}}{dN}\tag{4-13}$$

and,

$$\frac{da_{diss}}{dN} = \frac{i_{corr}}{zF\rho} M \frac{1}{\omega},\tag{4-14}$$

where  $da_{cf}/dN$ ,  $da_{air}/dN$ , and  $da_{diss}/dN$  represent the crack growth rates in a corrosive environment, in air, and due to metal dissolution, respectively. Also in above equations,  $i_{corr}$  is the anodic current density for metal dissolution,  $\omega$  the cyclic frequency,  $z$  the number of electrons,  $F$  Faraday's constant ( $9.64853 \times 10^4$  Coulombs / mole of electrons),  $M$  the molecular weight, and  $\rho$  the density. The modified model was validated through tests of a low alloy structural steel by Akid [1987]. The application of this modified model requires the information on microstructure of the material. More detailed discussion of these parameters is available in Akid [1987].

#### 4.5 Corrosion Models

In the context of time-dependent reliability analysis considering corrosion and fatigue, a corrosion model was proposed by Qin and Cui [2003] to better describe the corrosion process of steel structures subjected to corrosive environments. In the same reference, the authors compared their model to other existing corrosion models. Therefore the reference not only provides presumably a better corrosion model, it also provides references for other models for potential further exploration. The targeted material was mild and low alloy steels that are frequently used in marine environments for economical reason.

Qin and Cui [2003] also noted that a purely theoretical model, representing the loss of material due to corrosion, is extremely difficult to achieve because of the complexity of the actual corrosion mechanism. Most of the existing corrosion models are based on assumptions of the actual measurement. The proposed model by Qin and Cui [2003] attempted to better represent the actual corrosion process. This model assumes mild and low alloy steels immersed in marine environments. This assumption may correlate well with the internal environment of the service water systems in nuclear power plants where brackish water (i.e., adjacent to ocean water) is used as the source of cooling water.

Prior to this model, the models have not considered well the effect of the corrosion protective system (CPS), e.g. paint coating or cathodic protection [Southwell et al, 1979, Melchers, 1995-1999, Paik et al, 1998, Guedes Soares and Garbatov, 1999]. This model divides the corrosion process into three stages with an indicator variable  $q$ : 1) no corrosion when CPS is fully effective  $q = 1, t \in [0, T_{st}]$ ; 2) corrosion accelerating when pitting corrosion starts and progresses,  $t \in [T_{st}, T_A]$ ; and 3) corrosion decelerating,  $q = 1, t \in [T_A, T_L]$ . In these expressions,  $T_{st}$ ,  $T_A$ , and  $T_L$  are the instant in time when pitting corrosion starts, corrosion accelerates (assumed to occur at the end of CPS life  $T_{cl}$ ), and the life of the structure ends or the structure requires repair, respectively. A Weibull function is utilized to describe the corrosion rate  $r(t)$  of this model,

$$r(t) = \begin{cases} 0, & 0 \leq t < T_{st} \\ d_{\infty} \frac{\beta}{\eta} \left( \frac{t - T_{st}}{\eta} \right)^{\beta-1} \exp \left\{ - \left( \frac{t - T_{st}}{\eta} \right)^{\beta} \right\}, & T_{st} \leq t \leq T_L, \end{cases} \quad (4-15)$$

in which  $d_{\infty}$ ,  $\beta$ ,  $\eta$ , and  $T_{st}$  are four parameters to be determined using methods provided by Qin and Cui [2003]. The maximum corrosion rate  $r_{\max}$  can be found at the time  $T_A$ ,

$$T_A = \begin{cases} T_{st} + \eta \left( \frac{\beta - 1}{\beta} \right)^{1/\beta}, & \beta > 1, \\ T_{st}, & \beta \leq 1 \end{cases} \quad (4-16)$$

and,

$$r_{\max} = \begin{cases} d_{\infty} \frac{\beta}{\eta} \left( \frac{\beta - 1}{\beta} \right)^{(\beta-1)/\beta} \exp \left( \frac{\beta - 1}{\beta} \right), & \beta < 1, \\ \frac{d_{\infty} \beta}{\eta}, & \beta = 1, \\ \rightarrow \infty, & \beta < 1. \end{cases} \quad (4-17)$$

Using this corrosion rate model, the reduction of thickness (loss of material) due to corrosion can be determined by the following resultant solution,

$$d(t) = \begin{cases} 0, & 0 \leq t < T_{st}, \\ d_{\infty} \left\{ 1 - \exp \left[ - \left( \frac{t - T_{st}}{\eta} \right)^{\beta} \right] \right\}, & T_{st} \leq t \leq T_L. \end{cases} \quad (4-18)$$

The proposed model is very flexible and can be used for many situations, by varying parameters  $d_{\infty}$ ,  $\beta$ ,  $\eta$ , and  $T_{st}$ . This model can be degenerated to various models in the literature by setting values for some of these parameters.

The model proposed by Guedes Soares and Garbatov [1999] can be obtained by setting  $\beta = 1$ , i.e.,

$$d(t) = d_{\infty} \left\{ 1 - \exp \left[ - \left( \frac{t - T_{st}}{\eta} \right) \right] \right\}. \quad (4-19)$$

The model proposed by Paik, et al [1998] can be obtained by setting  $\eta = 1$  and taking only the linear term of the Taylor expression of  $d(t)$ :

$$d(t) = d_{\infty}(t - T_{st})^{\beta}. \quad (4-20)$$

Setting  $d_{\infty} = 0.1207$ ,  $T_{st} = 0$ , and  $\beta = 0.6257$  in the Paik's model as shown above yields the model developed by Melchers [1999],

$$d(t) = 0.1207t^{0.6257}. \quad (4-21)$$

The application of the Weibull function based model requires the determination of four parameters, which Qin and Cui [2003] provided two methods involving nonlinear regression for this purpose. The first method treats the four parameters as deterministic while the second method assumes they are random. These two methods are conceptually simple and the relevant details can be found in Qin and Cui [2003].

Table 4-1 Average Values for Corrosion Parameters  $C$  and  $\alpha$  [Albrecht and Naeemi, 1984].

Environment	Carbon Steel		Weathering Steel	
	$C$	$\alpha$	$C$	$\alpha$
Rural	34.0	0.65	33.3	0.50
Urban	80.2	0.59	50.7	0.57
Marine	70.6	0.79	40.2	0.56

## 5 DEGRADATION MODELS FOR STAINLESS STEEL

Three degradation models have been identified for stainless steel, which are potential useful in the environment of NPPs and are envisioned to be applicable to time-dependent fragility analysis. The first model is a computer-simulation based model consisting of a crack growth model and a fatigue crack model. The second model is a time-dependent fatigue damage model that considers the impact of strain rate on the fatigue damage of the stainless steel at elevated temperatures. The third model has a thorough theoretical background which considers the mechanochemical aspects of stress corrosion cracks, and has a relatively simpler and more appreciable numerical version.

Sections 5.1 through 5.3 provide descriptions of the time-dependent degradation models for stainless steel materials. It should be noted that these descriptions provide a summary of the degradation models and present the fundamental equations along with the key parameters used to define the degradation. For further information and proper implementation of these models, the references cited should be utilized. For the convenience of notation, some models are designated as the name of the leading author that the referenced model was reviewed, but not necessarily as the first person who developed the model.

### 5.1 Machida's Model

In assessing various computer codes to estimate the reliability of piping with flaws due to stress corrosion cracking (SCC), Machida, et al [2008] described a set of methods in modeling of the SCC cracks of austenitic stainless steel piping. This effort was conducted in order to address the numerous observed SCC cracks in the weld joints of pipes in the primary loop recirculation systems (PLR) in BWR operating in Japan. This model is a blend of several sub-models, which also include the contribution from fatigue. This model is simulation based.

#### 5.1.1 Model for Crack Initiation

The crack initiation is simulated by a random generator, so are crack length, circumferential location, and the distance from the weld. The distributions of these random variables can be any of the uniform, normal, lognormal, and exponential distributions. The crack depth is assumed to be constant (usually 0.5 mm).

#### 5.1.2 Crack Growth Models

The crack growth rate due to SCC is in the form of the power model, i.e.,

$$\frac{da}{dt} = CK^m, \quad (5-1)$$

where  $K$  is the stress intensity factor, the coefficient  $C$  is determined by a random number generator, and  $m$  is a constant. The base metal and the weld have different parameters  $C$  and  $K$ ; when a crack propagates from the base metal into the weld material, a switch of these parameters is needed.

This model also considers the crack growth rate due to fatigue, which is expressed as,

$$\frac{da}{dN} = C_F t_r^{0.5} \Delta K^{3.0} (1 - R)^{2.12}, \quad (5-2)$$

Where  $\Delta K$  is the range of the stress intensity factor,  $C_F$  a deterministic coefficient,  $R$  the stress ratio, and  $t_r$  the loading time of a transient. The crack growth rate due to fatigue is significantly less than that due to SCC.

Two cracks are combined into one single crack when they grow into each other. The depth of the combined crack is the larger of the depths of the two cracks, and the length of the combined crack is the summation of the two cracks. When the length of a crack exceeds the inner circumference of the pipe, the crack is treated as a circumferential crack.

The dimensions of the crack (depth and crack angle) are implemented in the allowable bending stress formulation to determine the stability of the pipe section. This step is the same as the structural models described previously for the purpose of assessing the structural strength of degraded components.

## 5.2 Time-Dependent Fatigue Damage Model

Experimental data have shown that fatigue life at elevated temperature is affected by the shape of the loading cycles and strain rates, making the fatigue life prediction beyond the purely cycle based formula that have been described previously. The cyclic life with fast (F)-slow (S) loading (for loading-unloading) are less than that with F-F loading; the cyclic lives with S-F and S-S load are substantially smaller than that with F-F loading. Sun, et al. [2008] formulated a composite model for the time-dependent fatigue damage without hold-time, and validated the formulation using specimens of materials 2.25Cr-1Mo steel (mostly for boilers and heat exchangers) and 304 stainless steel. The proposed model considers the time-dependent damage under cyclic loading without hold time at elevated temperatures with a computing time defined as,

$$t_c = t_t \left( \frac{\dot{\epsilon}_c}{\dot{\epsilon}_t} \right)^\gamma, \quad (5-3)$$

where  $t_c$  is the computing time for time-dependent damage during one cycle,  $t_t$  the tension time during one cycle,  $\dot{\epsilon}_t$  and  $\dot{\epsilon}_c$  are the loading and unloading strain rates during one cycle,  $\gamma$  a factor to consider the influence of strain rate, which can be determined by fitting uni-axial test data from tests with symmetrical and asymmetrical loadings.

The effective total fatigue damage  $D$  is defined by a summation of three terms,

$$D = D_f + D_{cf} + D_c, \quad (5-4)$$

where  $D_f$  is the pure fatigue damage,  $D_c$  the time-dependent damage caused by time-dependent factors at elevated temperature, and  $D_{cf}$  the interaction damage between time-dependent factors and pure fatigue. When the total damage  $D$  reaches unity (1), fatigue failure occurs.

The three damage terms  $D_f$ ,  $D_c$ , and  $D_{cf}$  are defined as,

$$\begin{aligned} D_f &= \frac{n}{N_f}, \\ D_c &= \sum_{i=1}^n \frac{t_c}{t_r}, \\ D_{cf} &= \left( \sum_i \frac{t_c}{t_r} \times \frac{n}{N_f} \right)^\alpha, \end{aligned} \quad (5-5)$$

in which  $n$  is the number of the time-dependent fatigue cycles,  $N_f$  the pure fatigue life,  $t_r$  the creep time to rupture at one-half of the peak stress value, and  $\alpha$  an interaction factor between time-dependent damage and pure fatigue damage, which can be determined by fitting the uni-axial test data from tests with symmetrical and asymmetrical cyclic loadings. One-half of the peak stress value  $\sigma_c = \sigma_{\max}/2$  is considered to be the creep stress for steady cyclic loading conditions. The creep time to rupture  $t_r$  can be determined by utilizing the stress-creep time curve and the creep stress.

Using experimental data by Inoue, et al. [1989] that involved uni-axial fully reversed strain-controlled test of 2.25Cr-1Mo steel at 600 °C in air,  $\gamma$  was found to be 0.180 and  $\alpha$  was 0.434. The errors using this model were within a factor of 1.5 to 1.8. Similar tests with multi-axial loadings at 600 °C in air by Inoue, et al. [1994] were also utilized in verification of this model. The strain rate influence factor  $\gamma$  and the interaction factor  $\alpha$  were taken as the values from the uni-axial tests. The errors in the prediction using the model were mostly within a factor of 1.5. The fast strain rate was 0.5%/s and the slow strain rate was 0.01%/s for both groups of tests. The time-dependent damage was found to be about 9% of the total damage for S-F and S-S loadings and about 2% for the F-S loading; while the interactive damage was about 20% of the total damage.

Uni-axial tests of AISI 304 stainless steel at 593 °C [Majumdar and Maiya, 1978, Ermi and Moteff, 1983] were also used to validate the model. The tests were conducted with a servo-controlled hydraulically actuated fatigue machine. The strain rate influence factor  $\gamma$  and the interaction factor  $\alpha$  were determined using the test results to be 0.2855 and 1.2895, respectively. The errors in the prediction were within a factor of 2. The multi-axial test data by Zhang, et al. [2007] were used; however the test temperature was 600 °C, slightly higher than the uni-axial tests. Using the parameters  $\gamma$  and  $\alpha$  determined above (0.2855 and 1.2895), the errors in the prediction were within a factor of 2.5; a larger error range may be due to the differences of these tests in material chemical contents and specimen shapes and the absence of stress information in Zhang et al. [2007].

This model is considered to be suitable for situations of low-cycle fatigue at elevated temperature for stainless steel and 2.25Cr-1Mo steel.

### **5.3 Mechanochemical Model for SCC in High Temperature Water**

Saito and Kuniya [2001] recently developed a mechanochemical model to predict the SCC growth of stainless steel submerged in 288 °C water. This model is useful because austenitic stainless steel (especially type 304) is widely used in light water reactors (LWRs), and the structural integrity of the involved components due to intergranular stress corrosion cracking (IGSCC) is often a concern in NPPs. The authors also noted that the importance of understanding the SCC crack growth lies in the longer operating life expectation of the NPPs due to economic reasons.

This SCC crack growth model for type 304 stainless steel is based on a hypothesis of the slip-formation/dissolution mechanism and is expressed as a function of material conditions, water chemistry, and stress related parameters. This model involves two major mechanisms: 1) slip step formation due to dislocation movement at the crack tip, and 2) anodic dissolution at the bare surface after the slip deformation. The derivation of this model was lengthy, highly theoretical, and beyond the capability of common structural engineers. Interested readers are recommended to refer back to the original reference. Fortunately, based on the theoretical development, the authors developed relatively simple numerical models for type 304 stainless steel in 288 °C water, using a minimal number of parameters.

The relatively simplified model of the SCC crack growth rate can be represented by the following simple power law,

$$\frac{da}{dt} = A_0 \left( \frac{\dot{\epsilon}_{ct}}{C_m} \right)^n, \quad (5-6)$$

in which  $A_0$  is the rate coefficient,  $\dot{\epsilon}_{ct}$  the crack tip strain rate,  $C_m$  the material factor constant, and  $n$  the numerical constant that is a function of the degree of sensitization, water conductivity, and corrosion potential.

The rate coefficient  $A_0$  may be expressed (theoretically) as a number of parameters including anodic current density, atomic weight of the steel, metal density, and the number of electrons involved in the reaction rate, etc. However, Saito and Kuniya [2001] was able to use data in the literature to reduce this parameter for the particular case of stainless steel in 288 °C water into an elegant constant,

$$A_0 = 1.1 \times 10^{-7}. \quad (5-7)$$

The crack tip strain rate  $\dot{\epsilon}_{ct}$  is theoretically expressed as a very complicated formulas involved with 16 parameters. In the case of type 304 stainless steel at 288 °C,  $\dot{\epsilon}_{ct}$  is simplified (with a few numerical constants) to,

$$\dot{\epsilon}_{ct} = 1.1 \times 10^7 \exp \left( - \frac{3 \times 10^{-19} - 1.5 \times 10^{-20} (K - 9)^{1/3}}{7.74 \times 10^{-21}} \right), \quad (5-8)$$

in which  $K$  is the applied stress intensity factor ( $\text{MPa}\sqrt{\text{m}}$ ). It is noted by the authors that the scattering of the test data can be over two orders of magnitude, however the agreement between the model and test data is considered to be fair good.

The material factor constant  $C_m$  also involves quite a few other parameters in its theoretical form. Using data for type 304 stainless steel and a particular dislocation density,  $C_m$  becomes a constant,

$$C_m = 4.4 \times 10^{-4}. \quad (5-9)$$

Combining these parameters, the SCC crack growth rate then becomes a function of  $K$  and  $n$  only, as expressed by the following equation,

$$\frac{da}{dt} = 1.1 \times 10^{-7} \left[ 2.5 \times 10^{10} \exp \left( - \frac{3 - 0.15(K - 9)^{1/3}}{0.0774} \right) \right]^n \quad (5-10)$$

In which  $K > 9 \text{ MPa}\sqrt{\text{m}}$ .

The numerical constant  $n$  can be expressed as,

$$n = -\frac{1}{3} \{ \ln[(1 + C_1 \text{EPR})(C_2\kappa + C_3)(C_4\phi_C + C_5)] + C_6\phi_C + C_7 \}, \quad (5-11)$$

Where EPR is the electrochemical potential kinetic reactivation,  $\kappa$  the bulk water conductivity, and  $\phi_C$  the bulk corrosion potential,  $C_1$ - $C_7$  are numerical constants, which are determined from a database of test data using a wide range of stressing ( $11 \text{ MPa}\sqrt{\text{m}} \leq K \leq 60 \text{ MPa}\sqrt{\text{m}}$ , material ( $1.4 \text{ C/m}^2 \leq \text{EPR} \leq 13 \text{ C/m}^2$ ), and water chemistry ( $0.1\mu\text{S/cm} \leq \kappa \leq 1.5\mu\text{S/cm}$ ,  $-280\text{mV} \leq \phi_C \leq 250\text{mV}$ ). The values of  $C_1$ - $C_7$  are given as,

$$\begin{aligned}
 C_1 &= 3.57 \times 10^{-2}, \\
 C_2 &= 1.49 \times 10^{-8}, \\
 C_3 &= 2.23 \times 10^{-8}, \\
 C_4 &= 4.57 \times 10^{-3}, \\
 C_5 &= 23.12, \\
 C_6 &= 2.29 \times 10^{-3}, \\
 C_7 &= 11.56.
 \end{aligned}
 \tag{5-12}$$

To summarize, the model of the SCC crack growth rate really only has four parameters:  $K$ , EPR,  $\kappa$ , and  $\phi_C$ . As for application to type 304 stainless steel in 288 °C water, the ranges (or typical values) of these four parameters as described in Saito and Kuniya [2001] are shown below,

$$\begin{aligned}
 K &= 28 \text{ MPa}\sqrt{\text{m}}, \text{ depends on loading} \\
 \kappa &= 0.1 - 1.2 \mu\text{S/cm} \\
 \text{EPR} &= 6 - 13 \text{ C/cm}^2 \\
 \phi_C &= -200 - +250 \text{ mV}.
 \end{aligned}
 \tag{5-13}$$



## 6 OBSERVATIONS AND CONCLUSIONS

This report presents a summary of the Year 2 research, the second part of the five year BNL-KAERI collaboration program to support KAERI in its development of seismic capability evaluation technology for degraded structures and components in nuclear power plants (NPPs). The goal of the Year 2 task was to identify time-dependent degradation models to represent the long-term behavior of dominant materials used in NPPs, which have strong dependency on the component type, material, environment, and loading. The identified age-related degradation models may be used in conjunction with probabilistic risk assessments (PRAs) to estimate the time it would take for degradation of a component to introduce significant risk to a NPP.

It is recognized that the age-related degradations of structures and passive components (SPCs) are highly complex processes and can be extremely difficult to develop models that encapsulate all or most of the affecting factors. It is also prohibitive to develop/identify degradation models for all SPCs. To this end, Section 2 of this report presents a scoping study for the risk-significant components and the related dominant materials, by combining the Year 1 research results on degradation occurrences for the 10 preselected categories of SPCs using recent publicly available information sources, NUREG/CR-6679, and a particular review of license renewal applications (LRAs). It is concluded that exchangers, piping systems, RPVs, tanks, anchorages, and concrete are risk-significant component categories. The dominant materials for these components are identified as concrete, carbon and low-alloy steels, and stainless steel. Sections 3 through 5 summarize the identified degradation models for these materials.

Section 3 presents five age-related degradation models applicable to concrete material. It also includes a general discussion of the relation between concrete crack characteristics and reinforcement corrosion, a fundamental relation that is common to all degradation models for reinforced concrete. Introduced in a study of reliability-based service life prediction, the power model represents the depth of attack or deterioration as a power function of time after the deterioration process is initiated. Methods to calculate the required deterioration initiation time, deterioration rate, and the order of the power are also provided. The Thoft-Christensen's model and the Basheer's model are both based on Fick's law of diffusion in representing the chloride transport process, the latter of which also includes the mass conservation in the formula. Sarvewaran's model is a linear corrosion model for the loss of cross section area of a rebar, and was used in reliability analysis of deteriorating structures. Marsh's model was used in development of a reliability model for use in structural health monitoring, which features a general corrosion model and a pitting corrosion model for the reinforcement. These material degradation models can be incorporated into a structural model to obtain the structural resistance of a degraded component, where the structural model is component and limit state dependent.

Section 4 of this report describes five degradation models for carbon and low-alloy steels. The power model included as the first model in this section is the same as that described above for the concrete material, with parameters experimentally determined for various environments. The Henshall's model is a dry oxidation model for iron and low-carbon steels at moderately elevated temperature. This model represents the thickness of  $Fe_3O_4$  as a parabolic relation to the exposure time, in which the parameters were derived from experiments. The fatigue crack growth models are suitable for high cycle fatigue, in which the instantaneous crack growth is modeled as a function of the cyclical component of the stress intensity factor. These models have both deterministic and stochastic formats. The cycle life in these models can be directly related to service time once the loading history is known. The corrosion-modified fatigue growth model considers the fatigue growth of a component when it is in an aggressive environment and corrosion occurs simultaneously with fatigue. Corrosion can significantly reduce the fatigue life.

The last model identified in this section is the corrosion model for mild or low alloy steel that is immersed in marine environment, which is similar to the internal environment of some service water systems in NPPs. This model is very powerful and flexible and can be degenerated to various models in the literature by assigning certain values to some of these parameters.

Section 5 provides a summary of three degradation models for stainless steel. Machida's model was initially developed to assess various computer codes for estimation of the reliability of austenitic stainless steel piping having flaws due to stress corrosion cracking (SCC). This model combines several sub-models, which include a power law crack growth model due to SCC and also a sub-model to include the fatigue crack growth. This model is simulation-based, and can combine in the simulation two cracks into one when they grow into each other. The time-dependent fatigue damage model can be used in situations where elevated temperature and varied shapes of loading cycles exist. The damage measure is based on the utilization of loading cycle capacity. This model was validated using 2.25Cr-1Mo steel and 304 stainless steel, and is targeted at low-cycle fatigue. The mechanochemical model was developed to predict the SCC growth of stainless steel submerged in 288 °C water. This model is useful because austenitic stainless steel (especially type 304) is widely used in light water reactors (LWRs). The description of this model in this report omits the lengthy and highly theoretical derivation but focuses on the simplified experimental model for the sake of practical application. The simplified model is represented by a power law, with four key parameters determined using experimental data for type 304 stainless steel in 288 °C water.

This report represents the best effort in identifying and reviewing relevant age-related degradation models for the dominant materials used for selected risk-significant SPCs. All of the reviewed documents are from publicly available sources. These models are intended for consideration when performing fragility analysis of SPCs for the Year 3 and 4 tasks. However, as discussed in this report, the number and complexity of the time-dependent degradation models can be very significant due to the very large number and types of components in the NPPs, varied environmental conditions, differing failure modes, and the risk significance of their failures. Therefore, depending on the particular SPC and its risk significance, additional degradation models may need to be identified to incorporate aging of the component in a fragility analysis. This report is useful to identify some of the common degradation models, serve as guidance on selection of appropriate models, and also provides an extensive list of references that are useful for searching of additional models. It is emphasized here that the description of the models in this report is aimed at providing concise summaries about the models and the corresponding applicability in fragility analysis, however, the actual application of these models in fragility analysis should refer back to the original references for model implementation and parameter determination.

## 7 REFERENCES

Akid, R. (1987). "The initiation and growth of short fatigue cracks in an aqueous saline environment." Ph.D. thesis, University of Sheffield, UK.

Akid, R. and Miller, K.J. (1991). "Short fatigue crack growth behavior of a low carbon steel under corrosion fatigue conditions." *Fatigue & Fracture of Engineering Materials and Structures*, **14**(6), 637-649.

Albrecht, P. and Naeemi, A.H. (1984). "Performance of weathering steel in bridges." Report 272, Nat. Cooperative Highway Res. Program.

Alonso, C., Andrade, C., Rodriguez, J., and Diez, J.M. (1998) "Factors controlling cracking of concrete affected by reinforcement corrosion." *Materials and Structures* **31**(211), 435-441, RILEM, Cachan, France.

Andrade, C., Alonso, C., and M. Molina, F. (1993). "Cover cracking as a function of bar corrosion: part 1 – experimental test." *Materials and Structures* **26**(162), 453-464, RILEM, Cachan, France.

Barsom, J.M. and Rolfe, S.T. (1987). *Fracture and Fatigue Control in Structures*. Prentice Hall Inc, Englewood Cliffs, NJ.

Basheer, P.A.M., Chidiac, S.E., and Long, A.E. (1996). "Predictive models for deterioration of concrete structures." *Construction and Building Materials*, **10**(1), 27-37.

Bertolini, L., Elsener B., Pedferri, P., Polder R. (2004). *Corrosion of Steel in Concrete*. Wiley-VCH, Weinheim, Germany.

Beeby, A.W. (1978). "Corrosion of reinforcing steel in concrete and its relation to cracking." *The Structural Engineer* **56A**(3), 77-81, London, United Kingdom.

Beeby, A.W. (1979). "Corrosion of reinforcement and crack widths." *Proceedings of International Symposium, Offshore Structure*, 1.47-1.60, Rio de Janeiro, Brazil, Pentech Press, Plymouth, United Kingdom.

Braverman, J.I., Miller, C.A., Ellingwood, B.R., Naus, D.J., Hofmayer, C.H., Shteyngart, S., and Bezler, P. (2001). "Probability-based evaluation of degraded reinforced concrete components in nuclear power plants." NUREG/CR-6715, Brookhaven National Laboratory.

Cady, P.D. and Weyers, R.E. (1984). "Deterioration rates of concrete bridge decks." *Journal of Transportation Engineering* **110**(1), 35-44, American Society of Civil Engineers, New York.

Cliff, J.R. and Knab, L.I. (1989). "Service life of concrete." National Bureau of Standards (now NIST), NUREG/CR-5466, U.S. Nuclear Regulatory Commission, Washington D.C.

Ellingwood, B.R., and Song, R. (1996). "Impact of structural aging on seismic risk assessment of reinforced concrete structures in nuclear power plants." NUREG-CR-6425, The Johns Hopkins University/Oak Ridge National Laboratory.

- Ermi, A.M. and Moteff, J. (1983). "Microstructural development and cracking behavior of AISI 304 stainless steel tested in time-dependent fatigue modes." *Journal of Engineering Materials and Technology*, **105**, 21-30.
- Francois, R. and Arliguie, G. (1999). "Effect of microcracks and cracking on the development of corrosion in reinforced concrete members." *Magazine of Concrete Research* **51**(2), 143-150, London, United Kingdom.
- Funahashi, M. (1990). "Predicting corrosion-free service life of a concrete structure in a chloride environment." *ACI Material Journal*, November/December, 581-587.
- Goltermann, P. (1994). "Mechanical predictions on concrete deterioration. Part I: Engenstresses in concrete." *ACI Material Journal*, **91**(6), 543-550.
- Guedes Soares, C. and Garbatov, Y. (1999). "Reliability of maintained, corrosion protected plates subjected to nonlinear corrosion and compressive loads." *Marine Structures*, **12**, 425-445.
- Henshall, G.A. (1996). "Numerical predictions of dry oxidation of iron and low-carbon steel at moderately elevated temperature." *Materials Research Society Fall Meeting*, Boston, MA.
- Hobson, P.D., Brown, M.W., and de los Rios E.R. (1986). "Two phases of short crack growth in a medium carbon steel." *The Behavior of Short Fatigue Cracks EGF1*, Edited by Miller, K.J. and de los Rios, E.R., MEP Inst. Mech. Engrs, London, 441-459.
- Ida, A. and Yokomuro, T. (1987). "Durability survey of 60 year old reinforced concrete office building." Annual Meeting, Architectural Institute of Japan, Tokyo, 1987.
- Inoue, T., Igari, T., Okazaki, M., et al. (1989). "Fatigue-creep life prediction of 2¼ Cr-1Mo steel by inelastic analysis." *Nuclear Engineering and Design*, **114**, 311-321.
- Inoue, T., Kishi, S., Koto, H., et al. (1994). "Fatigue-creep life prediction of 2¼ Cr-1Mo steel under combined tension-torsion at 600 °C." *Nuclear Engineering and Design*, **150**, 119-127.
- Li Y., Vrouwenvelder T., and Wijnants G.H. (2003). "Spatial Variability of Concrete Degradation." *Life-Cycle Performance of Deteriorating Structures*, Editors: Frangopol, D.M., Bruhwiler, E., Faber, M.H., and Adey, B. ASCE.
- Liu, Y. and Weyers, R.E. (1998). "Modeling of the time to corrosion cracking in chloride contaminated reinforced concrete structures." *ACI Materials Journal*, **95**, 675-681.
- Machida, H., Arakawa, M., Yamashita, N., and Yoshimura, S. (2008). "Study on probabilistic fracture mechanics analysis codes for pipes with stress corrosion cracks." *Proceedings of the 16<sup>th</sup> International Conference on Nuclear Engineering (ICONE16)*, May 11-15, Orlando, Florida.
- Majumdar, S. and Maiya, P.S. (1978). "Waveshape effects in elevated-temperature low-cycle fatigue of type 304 stainless steel." *Inelastic Behavior of Pressure Vessel and Piping Components*, PVP-PB-028, New York, ASME, 43-54.
- Marsh, P.S. and Frangopol, D.M. (2008). "Reinforced concrete bridge deck reliability model incorporating temporal and spatial variations of probabilistic corrosion rate sensor data." *Reliability Engineering & System Safety*, **93**, 394-409.

- McAllister, T.P. and Ellingwood, B.R. (2001). "Evaluation of crack growth in miter gate welments using stochastic fracture mechanics." *Structural Safety*, **23**, 445-465.
- McDowell, D.L. (1996). "An engineering model for propagation of small cracks in fatigue." *Engineering Fracture Mechanics*, **56**(3), 357-377.
- Melchers, R.E. (1995). "Probabilistic modeling of marine corrosion of steel specimens." In *Proceedings of the ISOPE'95*, 12-15 June, Hague, Netherlands, 204-210.
- Melchers, R.E. (1997). "Modeling of marine corrosion of steel specimens." *Corrosion Testing in Natural Waters*, Editors Kain, R.M. and Young, W.T., Vol **2**, Philadelphia, ASTM STP 1300, 20-33.
- Melchers, R.E. (1998). "Probabilistic modeling of immersion marine corrosion." *Structural Safety and Reliability*, Editors Shiraishi, N., Shinozuka, M., and Wen, Y.K., Vol **3**, Rotterdam, Balkema, 1143-1149.
- Melchers, R.E. (1999). "Corrosion uncertainty modeling for steel structures." *Journal of Constructional Steel Research*, **52**, 3-19.
- Mori, Y. (2005). "Reliability-based service life prediction and durability in structural safety assessments." Chapter 7, *Structural Safety and Its Quality Assurance*, Editors: B.R. Ellingwood and J. Kanda, ASCE.
- Navarro, A. and de los Rios, E.R. (1988). "A microstructurally-short fatigue crack equation." *Fatigue & Fracture of Engineering Materials and Structures*, **11**, 383-396.
- Nie, J., Braverman, J.I., Hofmayer, C.H., Choun, Y.S., Kim, M.K., and Choi, I.K. (2008). "Identification and assessment of recent aging-related degradation occurrences in U.S. nuclear power plants." Annual Report for Year 1 Task. BNL Report-81741-2008, Brookhaven National Laboratory; KAERI/RR-2931/2008, Korean Atomic Energy Research Institute.
- NUREG-1522 (1995). "Assessment of inservice condition of safety-related nuclear plant structures." H. Ashar and G. Bagchi, U.S. Nuclear Regulatory Commission, Washington, D.C., June.
- Naus, D.J. (2007). "Primer on durability of nuclear power plant reinforced concrete structures – a review of pertinent factors." NUREG/CR-6927, Oak Ridge National Laboratory.
- Paik, J.K., Kim, S.K., Lee, S.K. (1998). "Probabilistic corrosion rate estimation model for longitudinal strength members of bulk carriers." *Ocean Engineering*, **25**(10), 837-860.
- Qin, S. and Cui W. (2003). "Effect of corrosion models on the time-dependent reliability of steel plated elements." *Marine Structures*, **16**, 15-34.
- Saito, K. and Kuniya, J. (2001). "Mechanochemical model to predict stress corrosion crack growth of stainless steel in high temperature water." *Corrosion Science*, **43**, 1751-1766.
- Sanzo, D., Kvam, P., Apostolakis, G., Wu, J., Milico, T., Ghoniem, N., and Guarro, S. (1994). "Survey and evaluation of aging risk assessment methods and applications." NUREG/CR-6157, Los Alamos National Laboratory.

- Sarveswaran, V. and Roberts, M.B. (1999). "Reliability analysis of deteriorating structures – the experience and needs of practicing engineers." *Structural Safety*, **21**(4), 357-372.
- Southwell, C.R., Bultman, J.D., Hummer Jr C.W. (1979). "Estimating of service life of steel in seawater." *Seawater Corrosion Handbook*, Editor Schumacher, M., New Jersey, Noyes Data Corporation, 374-387.
- Spencer B.F., Tang, J. and Artley, M.E., (1989). "Stochastic approach to modeling fatigue crack growth." *American Institute of Aeronautics and astronautics (AIAA) Journal*, **27**, 1628-1635.
- Stewart, MG (2004). "Spatial variability of pitting corrosion and its influence on structural fragility and reliability of RC beams in flexure." *Structural Safety*, **26**, 453-470.
- Thoft-Christensen, P. (2003). "Corrosion and cracking of reinforced concrete." *Life-Cycle Performance of Deteriorating Structures*, Editors: Frangopol, D.M., Bruhwiler, E., Faber, M.H., and Adey, B. ASCE.
- Tuutti, K. (1982). *Corrosion of steel in concrete*, Swedish Cement and Concrete Research Institute, Stockholm, CBI-research 4:82.
- Vesely, W.E. and Samanta, P.K. (1996). "Application of reliability degradation analysis." NUREG/CR-6415, Brookhaven National Laboratory.
- Vesikari, E. (1988). *Service life of concrete structures with regard to corrosion of reinforcement*. Research Reports, Espoo, Finland.
- Virkler, D.A., Hillberry, B.M. and Goel, P.K. (1978). "The statistical nature of fatigue crack propagation." *Journal of Engineering Materials and Technology*, **101**, 148-153.
- Washa, G.W. and Wendt, K.F. (1975). "Fifty-year properties of concrete." *Journal of American Concrete Institute*, **72**(1), 29-38.
- Washa, G.W., Saemann, J.C., and Crammer S.K. (1989). "Fifty-year properties of concrete made in 1937." *ACI Materials Journal*, **86**(4), 367-371.
- Yang, J.N. and Manning, S.D. (1996). "A simple second order approximation for stochastic crack growth analysis." *Engineering Fracture Mechanics*, **53**(5), 677-686.
- Zhang S.D., Harada, M., Ozaki, K., et al. (2007). "Multiaxial creep-fatigue life using cruciform specimen." *International Journal of Fatigue*, **29**, 852-859.
- Zheng, R. and Ellingwood, B.R. (1998). "Stochastic fatigue crack growth in steel structures subjected to random loading." *Structural Safety*, **20**(4), 305-324.